Journal Pre-proof

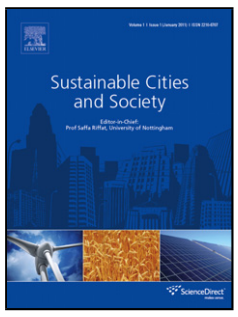

Supporting an integrated transportation infrastructure and public space design: A coupled simulation method for evaluating traffic pollution and microclimate

Liu Yang, Lufeng Zhang, Marc E.J. Stettler, Manlika Sukitpaneenit, Dunhui Xiao, Koen H. van Dam

PII: S2210-6707(19)30966-7

DOI: https://doi.org/10.1016/j.scs.2019.101796

Article Number: 101796

Reference: SCS 101796

To appear in:

Received Date: 16 April 2019

Revised Date: 9 August 2019

Accepted Date: 20 August 2019

Original Article

Supporting an integrated transportation infrastructure and public space design: A coupled simulation method for evaluating traffic pollution and microclimate

Liu Yang [1][0000-0002-3363-8620], [2], *, Lufeng Zhang [1], Marc E.J.Stettler [2], Manlika Sukitpaneenit [2], Dunhui Xiao [3], Koen H. van Dam [4][0000-0002-4879-9259], *

[1] Center of Architecture Research and Design, University of Chinese Academy of Sciences (UCAS).

[2] Centre for Transport Studies, Dept. of Civil and Environmental Engineering, Imperial College London.

[3] ZCCE, College of Engineering, Swansea University.

[4] Centre for Process Systems Engineering, Dept. of Chemical Engineering, Imperial College London.

* Corresponding authors

L. Yang: liu.yang1617@gmail.com

S403, Teaching Building, UCAS Zhongguancun Campus, Zhongguancun Nanyitiao 3Hao, Haidian Dist., Beijing, China.

K.H. van Dam: k.van-dam@imperial.ac.uk

453A, ACE Extension, South Kensington Campus, Imperial College London, London, UK.

Highlights

- A multiscale simulation method is presented for analyzing and evaluating transport infrastructure and public space urban designs.
- A mesoscale agent-based model, traffic emission models, and microclimate simulations are coupled to develop the modeling method.
- A two-fold evaluation is conducted, including mesoscale traffic-related emissions and the resulting air pollution at pedestrian level, in line with the microclimate of public open spaces and thermal comfort.
- An urban modeling-design framework is proposed and applied in a case study in Beijing.
- A holistic urban design strategy is helpful for achieving both an integration within the transport infrastructure and public space system and an external integration with the ecosystem.

- The findings are valuable for supporting urban designers and planners to build an environmentally- and pedestrian- friendly integrated transport infrastructure and public space plan.

Abstract

Traditional urban and transport infrastructure planning that emphasized motorized transport has fractured public space systems and worsened environmental quality, leading to a decrease in active travel. A novel multiscale simulation method for supporting an integrated transportation infrastructure and public space design is presented in this paper. This method couples a mesoscale agent-based traffic prediction model, traffic-related emission calculation, microclimate simulations, and human thermal comfort assessment. In addition, the effects of five urban design strategies on traffic pollution and pedestrian level microclimate are evaluated (i.e., a "two-fold" evaluation). A case study in Beijing, China, is presented utilizing the proposed urban modeling-design framework to support the assessment of a series of transport infrastructure and public space scenarios, including the Baseline scenario, a System-Internal Integration scenario, and two External Integration scenarios. The results indicate that the most effective way of achieving an environmentally- and pedestrian-friendly urban design is to concentrate on both the integration within the transport infrastructure and public space system and the mitigation of the system externalities (e.g., air pollution and heat exhaustion). It also demonstrates that the integrated blue-green approach is a promising way of improving local air quality, micro-climatic conditions, and human comfort.

Keywords

Multiscale model; Urban design; Traffic pollution; Microclimate simulation; Thermal comfort; Agent-based model.

1. Introduction

1.1. Background

Traditional transportation and urban planning paradigms emphasize maximizing the efficiency of motorized transport, which have caused negative impacts on urban environmental quality (De Nazelle et al., 2011). Motor vehicles have become a dominant contributor to local air pollution and a major risk for public health (Fenger, 1999; Su et al., 2015). In addition, massive transport infrastructure developments and a short of open spaces worsen the quality of the outdoor thermal environment and contribute to the urban heat island (UHI) effect. For instance, the annual air temperature in the center of Beijing rose 0.94 ˚C during the rapid urbanization from 1981 to 2000, almost three times of the heat rise from 1961 to 1980 (Ren et al., 2007). At a neighborhood scale, the car-oriented transport infrastructure construction also causes disconnected non-motorized transport networks and uncomfortable tracts of leftover public spaces (Anciaes et al., 2016; Carmona, 2003). Consequently, these outdoor spaces with deteriorated environmental quality, low walkability, and poor aesthetic design may discourage individuals from engaging in physical activities, especially walking (Chen & Ng, 2012; De Nazelle et al., 2011; Ewing & Cervero, 2010). Less active travel opportunities, in turn, increase auto-mobile usage, leading to heavier air pollution and heat emissions.

To break this vicious circle, there is a need for a new planning paradigm that prioritizes the needs of non-motorized travelers and the ecosystem by the design of an attractive, comfortable, and environmental-friendly *Integrated Transport Infrastructure and Public Space System* (Carmona, 2003; Cervero et al., 2017; Ravazzoli & Torricelli, 2017; United Nations, 2013). An integrated transport infrastructure and public space system, in this work, indicates that the urban spaces adjacent to transportation infrastructure are not an afterthought but are carefully designed as a public space network in parallel with the transport network. Such an integrated system, featuring human-centered and sustainable design, should encourage active travel, reduce pollution to the natural environment and be sensitive to local climate. To evaluate integrated system effectiveness, Heeres et al. (2016) distinguished three degrees of integration in a transportation project. As an analogous, the integration

levels in transport and spaces systems designs could be defined as *Functional Isolation* (no functional integration between transport and spaces), *System-Internal Integration*, and *External Integration.* System-Internal Integration means exploring problems within the transport and spaces system, while External Integration indicates addressing problems within a broader context (e.g., human systems, and the ecosystem) and aiming for the improvement of overall livability and sustainability in an area.

1.2. Literature Review

In this respect, many efforts have been paid to develop urban design and planning principles for creating integrated transport and spaces systems. Among others, five urban design strategies have been highlighted in literature (Kramer, 2013; Marchettini et al., 2014; Mueller et al., 2017; Shirehjini, 2016; Townsend, 2016; Woodcock et al., 2009) which are as follows: 1) mixed land-use and compact urban development, 2) accessible and connected street configuration with dedicated active travel infrastructures, 3) motorized transport emissions reduction, 4) climate-sensitive[1] urban public spaces, and 5) green and blue infrastructure provision. The first two approaches could only achieve System-Internal Integration, while the last three obtain External Integration with other urban systems, especially the ecosystem. More than anything else, green infrastructure is proved beneficial for mitigating UHI effects and transport emissions by using the filtering and absorption capability of trees and green buffer belts (Abhijith et al., 2017; Morakinyo & Lam, 2016). Additionally, Rozos et al. (2013) demonstrated that an integrated blue-green approach that provides high-quality water services in parallel with green spaces is even more effective than the sole use of “green” or “blue” infrastructure.

Many studies in recent years have focused on quantitative evaluation of the influence of these approaches on individuals, especially on pedestrians’ walking behavior. In doing this, computer modeling methods have been widely accepted as a key technique (Robinson, 2012). Martins et al. (2016) investigated the influence of resilient urban design strategies on outdoor climate and pedestrian thermal comfort; Du and Mak (2018) explored the influence on pedestrian level wind environment. Aschwanden (2014) and De Nazelle (2007) examined the impact of active travel plans

on local air pollution and walking behavior. Despite the knowledge acquired from all these studies, there is still a lack of research on evaluating the effectiveness of these approaches on building the integrated transport infrastructure and public space system.

According to De Nazelle et al. (2011), transportation infrastructure and public space plans impact individuals' travel mode choice, route choice, and physical activity. Besides, both plans have a direct link with environmental quality (e.g., air pollution, heat) that will further influence human behavior. Because motorized transport planning is usually undertaken at an urban scale/district scale, it has environmental impacts in this large scale too; whereas, its impact on individuals is most evident and direct at the pedestrian level. Urban public spaces (particularly those adjacent to infrastructures) design is typically performed at an urban block scale that may determine pedestrians' walking experience through affecting microclimate conditions and thermal sensation.In order to quantitatively assess the impact of various integrated transport and spaces plans on pedestrians and their physical activity (particularly walking behavior), this study aims at using computer simulations to perform a "two-fold" evaluation:

- urban scale traffic-related emissions and the resulting air pollution at pedestrian level;
- the microclimate of public open spaces and thermal comfort.

On the one hand, to assess road traffic emissions and the resulting local air pollution, a majority of studies introduced coupled modeling methods that combine traffic prediction models, emission calculations, and dispersion models (Borrego et al., 2003; Hatzopoulou & Miller, 2010). Generally, there are two ways for vehicle traffic estimation: one is using conventional aggregate models based on trips data, and the other is dis-aggregate Agent-Based Models (ABM) or activity-based models. In comparison with the aggregate approach, ABM gives insights of individual agents' behavior and how the agents interact with each other and with the different configurations of a built environment (Van Dam et al., 2013). ABM is also helpful for predicting impacts of individuals' decision on system-level outcomes such as the traffic (Waraich et al., 2009; Wise et al., 2017). In order to estimate vehicular emissions, numerous techniques were developed, which can be categorized into three types

according to their most appropriate scale of application (Smit et al., 2008). MEASURE, TEE, and COPERT are the most powerful tools in each type. Among others, COPERT is regularly applied in calculating traffic-related emissions on urban regions and small areas (ibid.). The measurement is performed based on traffic data and vehicular emission factors expressed as functions of average car speed (Gkatzoflias et al., 2007). Among the numerous pollution dispersion models such as Gaussian plume models and OSPM, Computational Fluid Dynamics (CFD) models are appropriate for small scale urban areas because CFD simulates air turbulence in a more sophisticated process (Vardoulakis et al., 2003).

On the other hand, there is considerable work involves evaluating the microclimate of open spaces using numerical models (e.g., Chokhachian et al., 2017; Shooshtarian et al., 2018). Four critical determinants of the outdoor microclimate are airspeed, air temperature, relative humidity, and mean radiant temperature. CFD models and MUKLIMO are common microclimate computational models. The condition of local microclimate can greatly influence pedestrian's thermal comfort[2], which has been assessed through a couple of indices such as the Predicted Mean Vote (PMV), Universal Thermal Climate Index (UTCI), and Physiological Equivalent Temperature (PET). Nasrollahi et al. (2017) used both PMV and UTCI to evaluate thermal comfort. To this end, several modeling techniques were developed to measure the degree of human's thermal satisfaction by considering the four microclimate factors and two personal parameters (i.e., clothing insulation and metabolic rate). ENVI-met and RayMan are the most frequently used models.

At a scale of open public spaces, ENVI-met (Bruse, 2002) is a powerful tool for modeling both microclimatic condition and thermal comfort (e.g., Chatzidimitriou & Yannas, 2016; Girgis et al., 2016; Salata et al., 2016). It is a three-dimensional prognostic model using CFD as a core process that is capable of simulating the surface-plant-air interactions in urban areas with a spatial resolution of 0.5—10m and a temporal resolution of 10 seconds. Although ENVI-met allows simulating the dispersion and deposition of multiple contaminants such as particles and gases through the embedded dispersion model, most of the literature uses measured traffic emission as input data (e.g., Morakinyo

& Lam, 2016; Wania et al., 2012). In this way, it is limited in predicting the air pollution under different transport network, land-use, and public space configurations which yield various traffic emission distributions. Despite the numerous investigations on estimating dynamic traffic emissions due to different urban layout, few studies considered both urban scale emissions, and pedestrian scale air pollution, microclimatic condition, and human comfort. Robinson (2012, p. 57) argued that "a way to overcome this problem is to couple different models capable of resolving different scales".

1.3. Research Objectives

To achieve the "two-fold" evaluation mentioned above, the novelty of this paper lies in proposing a multiscale simulation method to combine agent-based traffic simulation, vehicular emission calculations, microclimate simulations, and human thermal comfort evaluation. The spatial scales are defined as 1) mesoscale is 10km to 100km (e.g., urban districts), 2) microscale is less than 1km (e.g., city blocks), and 3) human scale is the individual body (Ooka, 2007).

In this study, microscale sites have been chosen for evaluating pedestrian level air quality, climate conditions, and thermal comfort. The acceptable walking distance of 400m (a 5-minute walk) is used to determine the range of sites (Aultman-Hall et al., 1997; Congress for the New Urbanism, 2000). In an attempt to capture local air quality in transport and spaces systems, this work considers the dynamic traffic emissions generated from mesoscale road transport. Thus, the research field is scaled up to include a mesoscale research segment and a buffer zone.

This paper, for the first time, presents a coupling framework to predict road traffic and related air pollution under mesoscale transport and spaces design proposals and to evaluate microscale air quality and climatic conditions. A realistic case in Beijing also demonstrates the urban modeling-design framework. Note, the suite of models is not expected to represent the complexity of the real urban environment entirely; it can offer assessments of and comparisons between various alternative design scenarios.

The remainder of the paper is organized as follows. Section 2 first describes the overall coupling simulation method and associated models, followed by a description of using this method as an urban

design support tool. Section 3 mainly demonstrates how the methodology is applied to Beijing to achieve a sustainable redesign of the vacated urban spaces in Beijing-Zhangjiakou (Jing-Zhang) High-Speed Rail (HSR) project. A series of urban design scenarios, including the *Functional Isolation scenario* (Baseline), *System-Internal Integration scenario* (Plan 0), and two *External Integration scenarios* (Plan 1 and Plan 2) are analyzed. Section 4 shows the simulation results, and discussions and conclusion are included in Section 5. The detailed explanation of algorithms and input parameters can be found in the Supplementary Data.

2. Methodology

This section presents the multiscale modeling approach proposed in this study, which involves four stages (see Fig. 1). In Figure 1, green boxes indicate the four modeling stages, parameters within gray boxes express the inputs of different models, and yellow boxes highlight the key modeling outputs studied in this research.

Stage 1: Agent-based modeling. ABM is used to predict traffic volume (cars on each road section in 24 hours a day) on a mesoscale baseline road network. The simulation result is then validated by comparisons with real-time data, after which the model is adjusted.

Stage 2: Traffic emission calculation. We compute the mass of air pollutants emitted by the cars simulated in ABM, and the result of hourly traffic emission $\boldsymbol{E}_{total}$ over the road network is then used for assessing transport and spaces plans. Afterward, $\boldsymbol{E}_{total}$ is converted to emission rates for importing to microsimulation. Among the range of traffic-induced pollutants, Nitrogen Oxides (NOx) is chosen as an example domain since road transport is the leading source of NOx emissions in urban areas. For example, mobile sources account for 71% of the total NOx emission in Beijing (Hao et al., 2000).

Stage 3: Microclimate simulation. We zoom into a microscale to model the impact of using different design strategies on pollutant concentration $\boldsymbol{C}^{*}$(in this case, refers to NOx concentration), airspeed, air temperature, relative humidity and mean radiant temperature. The emission rates yielded from the previous step and other required input files are imported into the simulation, keeping it consistent with the mesoscale.

Stage 4: Human thermal comfort assessment. The microsimulation results of pollution concentration and local climate conditions along with the personal parameters, are used for assessing pedestrian's thermal comfort through both PMV and UTCI indices.

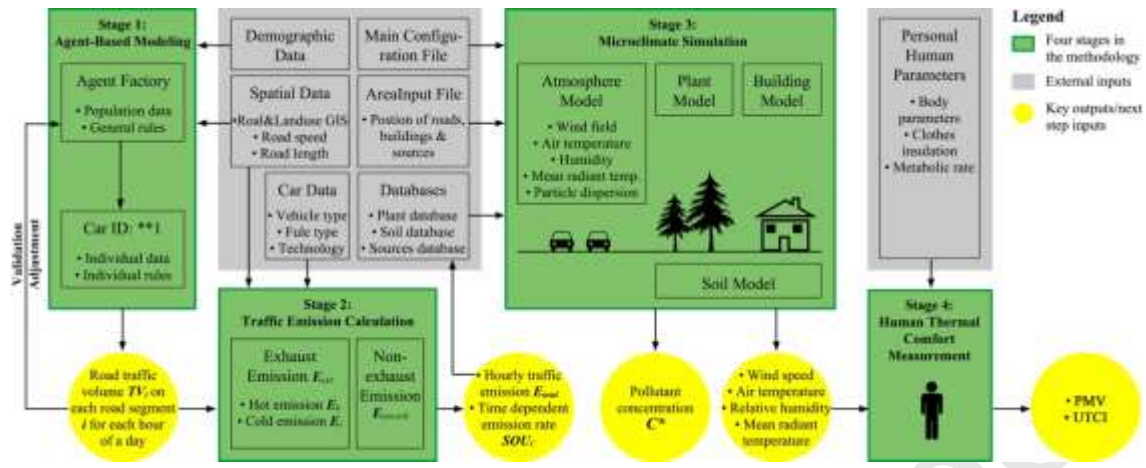

Figure 1. A multiscale simulation method for coupling ABM, Emission Calculation, Microclimate Simulation, and Thermal Comfort Assessment.

2.1. Agent-Based Modeling (ABM)

To capture the movement of cars, we adopt the Smart-City Model (Van Dam et al., 2017) which links an agent-based model of a synthetic population for a sample district with the spatial description of transport infrastructures and public spaces in Geographic Information System (GIS). Firstly, the real-world road network and land-uses (including residential areas, workplaces, public open spaces) of a mesoscale self-defined segment are represented as two separate layers. Subsequently, by using local socio-demographic data (i.e., population density, the ratio of workers/non-workers, household size and car-ownership) along with the location information of residential tracts, the model randomly generates car agents depending on the population density of residential areas.

Daily activity pattern $\boldsymbol{AP}_k$ is developed to generate a series of events with timestamps for worker agents (k_1) and non-worker agents (k_2) for capturing the diversity of activity schedules with relatively limited statistics around timing and occurrence (e.g., time use survey), that is (Eq.1),

$$\boldsymbol{AP}_k = \{(AT_j, MD_j, SD_j, PD_j)\} \quad \textbf{(Eq.1)}$$

where the activity type AT_j includes residential, industrial, commercial, leisure, or cultural activities. Each activity is determined by three parameters: 1) a mean departure time MD_j to represent the peak

hour of the departure period, 2) a standard deviation SD_j to simulate the variability in the departure time among agents, and 3) a probability of departure PD_j to account for agents that do not necessarily undertake certain trips. $\boldsymbol{AP}_k$ is generated by assuming no dependency between different activities and agents have no alternative choices during the same period (e.g., go to the park or go to shops at lunchtime). An example is given in the Supplementary Data (S1). These activities are also pre-defined in the land-use GIS layer.

To emulate individual route choice behavior, the original Smart-City Model applied the Dijkstra's shortest-path algorithm (Skiena, 1998), which could be found in the Supplementary Data (S2). After running for a Baseline scenario, we assess the quality of the results of traffic volume $\boldsymbol{TV}_i$ on each road segment i by comparing it with the realistic road usage data. In some calibration case studies, we found that the initial model cannot provide an accurate representation of the real-life traffic probably because the agents did not take account of traveling speeds when planning their routes. The validation outcomes in Beijing case study will be presented in Section 4. Thus, a significant improvement of this research is allowing the agents to consider the specific travel speed on each road when planning routes (roads of a higher hierarchy often have a higher speed). In other words, car agents use a quickest-path algorithm to choose routes (see Supplementary Data S3). When assigning speeds to the transport network, we first attached the design speed as a parameter to the road layer. Then the value was adjusted based on historical statistics and the real data for the sampling area.

2.2. Traffic Emission Calculation

Since the area chosen for this study is at a meso/urban scale, we use COPERT 4 to estimate on-road traffic emissions. The total air pollutant mass discharged from road transport $\boldsymbol{E}_{total}$ is calculated as a sum of exhaust pollutants $\boldsymbol{E}_{exh}$ (e.g., gases and particles) and non-exhaust pollutants $\boldsymbol{E}_{non\text{-}exh}$, which indicates the evaporation losses of the fuel system (European Environment Agency [EEA], 2016). For each road segment i, $\boldsymbol{E}_{exh}$ consists of hot emission $\boldsymbol{E}_{h,i}$ and cold-start emission $\boldsymbol{E}_{c,i}$ which occurs respectively after and before the vehicle subsystems have reached their normal operating temperature. These are measured based on Eq.2 and 3.

$$\boldsymbol{E}_{h,i} = e^h \times \boldsymbol{TV}_i \times L_i \quad \textbf{(Eq.2)}$$

$$\boldsymbol{E}_{c,i} = e^h \times (e^c/e^h - 1) \times \boldsymbol{TV}_i \times L_i \times \beta \quad \textbf{(Eq.3)}$$

where L_i is the length of road i. e^h indicates emission factors while e^c/e^h denotes the over-emission level compared to hot emission, and β is the fraction of mileage driven with a cold engine. The emission factors e^h are functions of vehicle types (fuel, emission standard, and capacity or weight) and the mean traveling speed. They are derived from the results of comprehensive scientific projects. This research uses the most recent COPERT e^h documented in the Air Pollutant Emission Inventory Guidebook (EEA, 2016). Inevitably, COPERT has limitations in using mean speed to estimate e^h and taking traffic jam into account only during model development. To minimize the possible inaccuracy, we ensured that the application of e^h is within the travel speed limits provided in the Guidebook and the applied case studies have relatively common driving conditions, e.g., not choosing traffic calming regulated places (Ntziachristos et al., 2000). Moreover, the length of each link in the road layer is more than 500m because the dependability of COPERT rises as the road link length rises above 400m (Samaras et al., 2014).

This simulation also reads the approved hourly traffic data $\boldsymbol{TV}_i$ yielded by the agent-based model. The model then outputs the hourly emissions $\boldsymbol{E}_{total}$ [g] of NOx on each road i. Having run for a Baseline scenario, COPERT also operates under the integrated mesoscale urban plans. The NOx emissions are later converted to time-dependent emission rates [mg/s•m] to be prepared as an input for the next step. Emission rate $\boldsymbol{SOU}_C$ for each hour of the day is calculated using Eq.4.1 (for line sources) and Eq.4.2 (for area sources).

$$\boldsymbol{SOU}_C = \boldsymbol{E}_{total-h}/(1000 \times 3600 \times L_i) \quad \textbf{(Eq.4.1)}$$

$$\boldsymbol{SOU}_C = \boldsymbol{E}_{total-h}/(1000 \times 3600 \times A_i) \quad \textbf{(Eq.4.2)}$$

where $\boldsymbol{E}_{total\text{-}h}$ is the total road traffic emission in an hour h [0-23] generated from COPERT. L_i the length of a road section i has a unit of [m], and A_i the area of a road crossing i has a unit of [m^2].

2.3. Microclimate Simulation

In order to quantify the impact of different transport and spaces designs on pedestrian-level air pollutant concentration and microclimatic conditions, we zoom into a microscale, selecting a research site within a 5-minute walk. The microclimate assessment is performed using ENVI-met 4 modeling technique, which is designed for this scale (Bruse, 2002). ENVI-met consists of four sub-models: the atmosphere model, the vegetation model, the soil model, and the building model (Bruse, 2007; Simon, 2016). The atmosphere model simulates the key processes in the microclimate: wind field, air temperature, humidity, radiative fluxes, turbulence, as well as pollutant dispersion and deposition. The non-hydrostatic three-dimensional Navier-Stokes formula is used for calculating wind speed. Air temperature and relative humidity are determined by the combined advection-diffusion equation considering internal sources and sinks. The same equation is harnessed for calculating the particle concentration $\boldsymbol{C}^*$ [mg/m^3] and can be written in Einstein summation as follows (Eq.5):

$$\frac{\partial C}{\partial t} + u_i \frac{\partial C}{\partial x_i} = \frac{\partial}{\partial x_i}\left(DIF_C \frac{\partial C}{\partial x_i}\right) + \boldsymbol{SOU}_C(x,y,z) + SED_C(x,y,z) \qquad \textbf{(Eq.5)}$$

where C indicates particle concentration [mg(C) /kg(Air)] which is converted to $\boldsymbol{C}^*$ [mg/m^3] for output. DIF_C and SED_C denote the diffusion coefficient and the sedimentation of pollutants, respectively. $\boldsymbol{SOU}_C$ describes local particle sources which are grouped into three types: point sources [mg/s], line sources [mg/s•m], and area sources [mg/s•m^2]. The cartesian coordinates $x_i = \{x, y, z\}$, and the corresponding wind speed vectors $u_i = \{u, v, w\}$.

2.4. Thermal Comfort Computation

Taking into account both the climatic parameters and the personal factors of clothing insulation and metabolic rate, we then analyze human thermal comfort through both PMV and UTCI indices. PMV evaluates thermal comfort of the whole microscale research site (1.5m above ground). At selected points of the site at the height of 1.5m, thermal comfort is assessed using UTCI. The calculation of PMV can be performed by the Bio-met module in ENVI-met directly while UTCI is

not a part of the model. Thus, we use the RayMan software to do the measurement, which is one-dimensional in space and time-independent (Matzarakis et al., 2007, 2010).

PMV was initially developed to rank the thermal (dis)comfort at different individual conditions within steady-state indoor situations (Fanger, 1972). In order to apply PMV to outdoor spaces, the index was adapted to include complex outdoor radiation (Jendritzky & Nübler, 1981) and was included in the International Organization for Standardization (ISO) standard (ISO, 1994). PMV can be calculated as follows (Eq.6):

$$PMV = [0.028 + 0.303 \times \exp(-0.036E_M)] \times (E_I - V_D - V_S - B_L - B_E - X_R - X_C) \quad \textbf{(Eq.6)}$$

with E_M as mechanical energy production of the body, while E_I as remaining internal energy which equals $E_I = E_M(1\text{-}\varphi)$, with φ meaning the mechanical work factor. V_D and V_S denote vapor diffusion through the skin, and evaporation of sweat on the skin, respectively. B_L and B_E indicate latent heat lost through breathing, and sensible heat gained/lost through breathing. X_R describes the radiative energy balance of the body, and X_C, the energy gained/lost through convection.

UTCI was initiated to create a universally valid index for outdoor thermal comfort assessments in various climates, seasons, and locations. The advanced Fiala multi-node thermoregulation model (Fiala et al., 2001) was selected to calculate the human physiological reaction to the outdoor climatic conditions, and an adaptive clothing model was developed and coupled (Havenith et al., 2011). UTCI[3] follows the concept of equivalent temperature and is very sensitive to changes in air temperature, solar radiation, humidity and particularly wind speed comparing to other indices including PMV (Blazejczyk et al., 2012). However, it is limited to accepting only a narrow range of input parameters, e.g., the valid wind speed ranges from 0.5 to 17m/s.

The scales of PMV could be classified in terms of thermal sensation, while the values of UTCI equivalent temperature are always categorized according to the grades of thermal stress. In Supplementary Data (Table S1), a comparison between PMV and UTCI and the thermal comfort zones of both indices are included.

2.5. Framework for Using the Coupled Simulation Method to Support Transport Infrastructure and Public Space Designs

A flow chart of using the coupled modeling approach to evaluate different transport infrastructure and public space plans is presented in Figure 2. Firstly, the Baseline scenario is analyzed and assessed by a series of Key Performance Indicators (KPIs), and then new plans are created aiming at achieving an integrated transport and spaces system. Afterward, the design alternatives pass through the same multiscale modeling process.

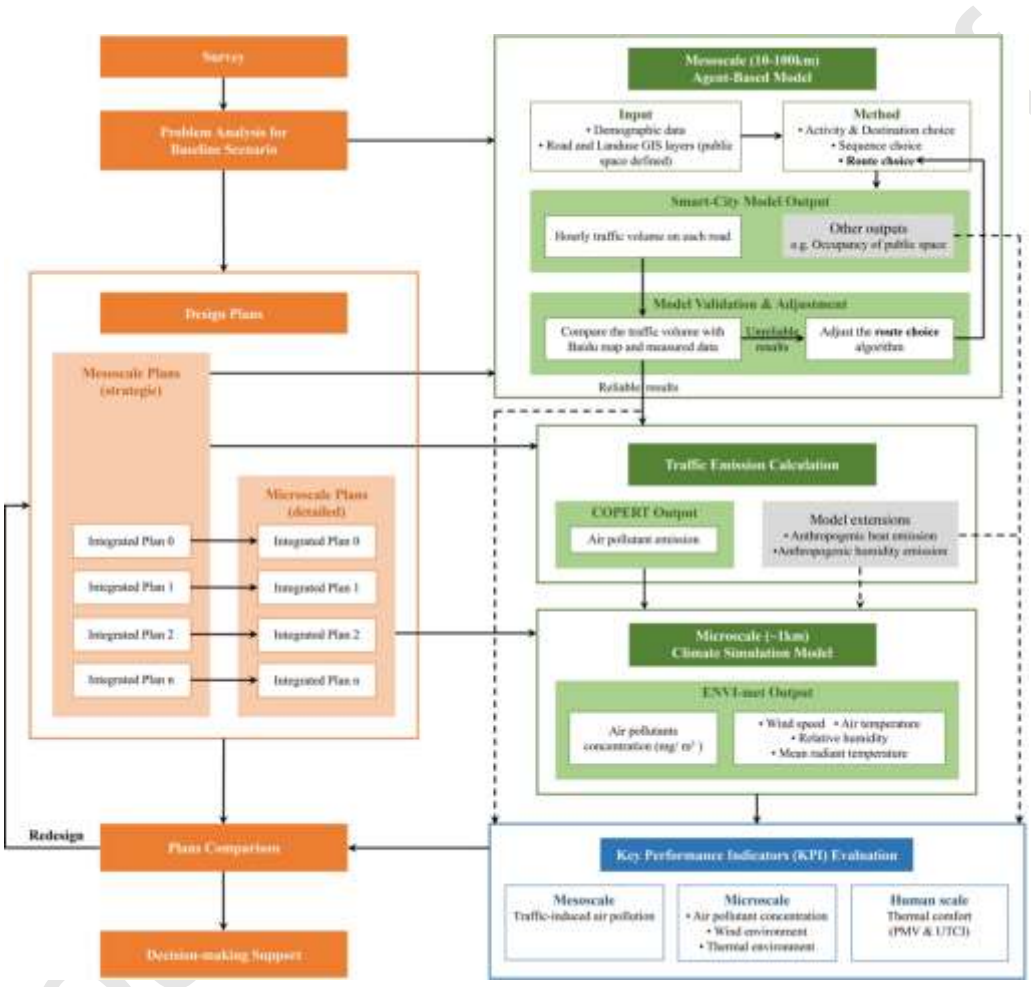

Figure 2. Framework for using the coupled simulation method to support transport infrastructure and public space designs (orange boxes indicate design processes, green ones are the coupled models, blue boxes contain evaluation KPIs, gray boxes and dash lines imply the potential framework extensions).

In this research, three types of KPIs are chosen: 1) mesoscale traffic-related air pollution, 2) pedestrian-level air pollutant concentration, wind, and thermal environment, and 3) human thermal comfort. Ultimately, a comparison of the KPIs of different scenarios can be used to support redesign and decision-making (plan selection). This allows making adjustments to the proposed plans or their overall design strategy, which could be re-evaluated, leading to an iterative development approach.

The design plans (geographical data inputs) used for different models are generated at different spatial scales. Mesoscale plans are drafted to choose overall design strategies and determine the spatial distribution of the transport network and land-uses. Microscale plans decide the detailed configuration of transport infrastructure and public spaces (e.g., the shape and size of pavements and water pools). For the sake of providing consistent evaluation results, the microscale plans in the framework are created based on the mesoscale plans.

Noteworthy, this framework has opportunities for evaluating other KPIs such as vehicle miles traveled and public space occupancy (by ABM), as well as anthropogenic heat and humidity emissions produced by cars. By extending the emission calculation model, heat emissions exhausted through fuel combustion in cars could be measured based on heat released by cars per meter, hourly traffic volume on each road segment, and the road length (Sailor & Lu, 2004). Besides, anthropogenic moisture generated from the combustion of fuel can be calculated through the mass of fuel burned in vehicles (Sailor, 2011).

3. Case study: Designing an Integrated Transport and Spaces System for the Jing-Zhang High-Speed Rail (HSR) project in Haidian District

The Jing-Zhang Railway is the first railway in China. In 2016, the government decided to demolish the old rail track and launched a smart Jing-Zhang HSR project in order to serve the 2022 Beijing Winter Olympics. Starting from Beijing North Railway Station in the northwest corner of the 2nd Ring Road, a new underground HSR passing through the city center was designed aiming to connect Beijing with the neighboring city Zhangjiakou. After removing the old rail, Beijing Municipal Commission of Planning and Natural Resources and related sectors have planned to sew the road network in Haidian District; however, urban designs for restructuring the urban spaces above ground are still in the air. The most recent governmental proposal is to transform these spaces into public open spaces. However, there is an urgent need for handling two issues which are also the motivation of this study: how to choose urban design strategies to transform the linear spaces, and how to enhance walking experience under new transport infrastructure and public space plans.

In this work, we apply the coupled modeling method to analyze the status quo transport and spaces system and test planned systems in terms of 1) mesoscale NOx emission distribution, 2) microscale NOx concentration, wind speed and air temperature, and 3) PMV and UTCI. As depicted in Figure 3, the mesoscale segment is chosen within a range of 800 meters to the underground section of the new HSR (10 km long), including a 2.5-3.0km buffer wrapped around the perimeter to avoid edge effects. Simultaneously, two sampling sites are selected for microscale analysis: one as a validation site with the availability of high-quality of data and the other a site which is directly affected by the proposed redevelopment under various design interventions. Site 1 covers a walkable area of 400m × 400m. Site 2 located in the middle of the railroad covering an area of 800m (400m either side of the rail) × 600m. Location and road network of the studied areas shown in Figure 4.

Figure 3. The microscale sites, mesoscale segment, and buffer zone delimited in this study.

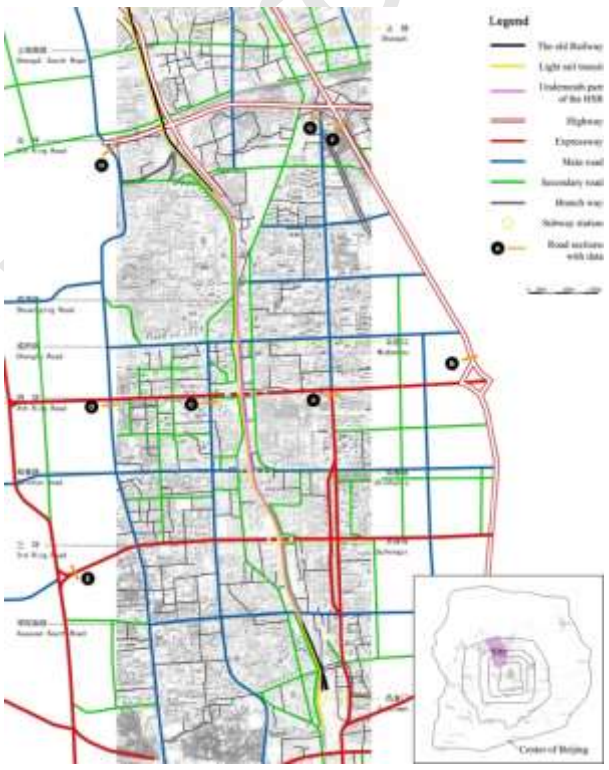

Figure 4. Location of the research site.

3.1. Agent-Based Modeling for Predicting Dynamic Traffic

3.1.1. Geographical data input

To construct the spatial environment in Smart-City Model, we import a GIS road file (an illustration in Fig. 4) which is a sampling segment drawn from the OpenStreetMap dataset (Geofabrik,

2017). A land-use file is extracted according to the parcel map for Beijing (ibid.) and the Points of Interests map (Long & Liu, 2013). The land-use layer is then modified to add the characteristics of human activities provided by each area (for the multi-use parts, the percent of each activity is assigned).

3.1.2. Socio-demographic data and activity schedule input

The 6th population census of Beijing (National Bureau of Statistics of China, 2010) is utilized for creating a synthetic population. We then assign a value of density to the residential land-uses in GIS by taking into account the socio-demographic data of Haidian District that describes the local demographic distribution, population density, the number of permanent residents, and the ratio of residential land-use. The number of private vehicles per person and the rate of worker/non-worker/visitors is extracted from (Beijing Haidian Yearbook Editorial Committee, 2017). Spatial-temporal activity patterns for workers, non-workers, and travelers are created based on the 2008 Time Use Survey in China (National Bureau of Statistics of China, 2008). In this survey, residents' activities are categorized into seven categories while they are summed up to five types in this simulation (for details see the paper (Yang et al., forthcoming)).

Here, we only simulate private cars whose activity patterns are the same as the residents' patterns. Other types of vehicles follow certain activity schedules that are out of the scope of this study (e.g., buses follow bus schedules). The simulated number of private cars is 80% of the total motor vehicles in Haidian District according to the statistics in (Beijing Transport Insitute, 2018).

3.1.3. Road speed data input

We first assigned the planned speed limit as a parameter to the road layer. Then the value was modified according to real-life data in Beijing: 1) a map of 2016 peak hour road network running speed (Beijing Transport Insitute, 2016), 2) statistics of 2017 peak hour road network running speed (Beijing Transport Insitute, 2017), and 3) average speed of the roads in the sampling area generated from a Didi taxi dataset. The results of average speed determination from Didi data show that the most frequency of mean speed on highway and expressway, main road, and secondary road are in the

range of 15-20, 10-15, and 8-13 [km/hr] respectively. These results are also compared with Zhang et al. (2017), the average speed on highway and expressway, and main road are consistent with their study (the mean speed calculation process and the outcomes are outlined in Supplementary Data S4).

3.1.4. Model Validation & Adjustment

After setting up the model for a baseline transport infrastructure and public space environment, the next step is to decide whether the modeled results resemble measured data; this is the so-called validation process. In this respect, the result of road usage frequency of the initial ABM using shortest-path is compared to Baidu Maps and the measured traffic volume of eight road sections (see the positions in Fig. 4). Afterward, we adjust the model to let the vehicle agents follow a quickest-path algorithm. To assess the reliability of the adjusted ABM, we compare the outputs of the quickest-path model and the shortest-path model with the real-life data. To measure how well the simulated traffic volume $\boldsymbol{TV}_{simulated}$ matches the corresponding measured amount $\boldsymbol{TV}_{measured}$, we introduce the Relative Error metric defined as (Eq.7):

$$Relative\ Error = (\boldsymbol{TV}_{simulated} - \boldsymbol{TV}_{measured})/\boldsymbol{TV}_{measured} * 100\% \quad \textbf{(Eq.7)}$$

here, a value of zero implies perfect modeling results, a value of 100% indicates the generated result is larger by a factor of two, and value of -100% means the result is smaller by a factor of two.

3.2. Mesoscale Urban Plan Scenarios

After validation, this study then uses the ABM to predict on-road traffic of a Functional Isolation scenario (Baseline), a System-Internal Integration scenario (Plan 0), and two External Integration scenarios (Plan 1 and 2). In the base case, land-uses adjacent to the old rail are mainly educational and residential with some pieces of commercial and leisure areas (see Fig. 5(a)). Public green spaces and the urban blue system (i.e., rivers and canals) are separated into pieces by the rail (see Fig. 5(b)). Furthermore, there are many dead-end roads near to the old rail. Similarly, walking and cycling infrastructures are disconnected and designed without considerations of human environmental comfort. An elevated light rail juxtaposed with the railway will continue to operate in the future which is kept in new designs.

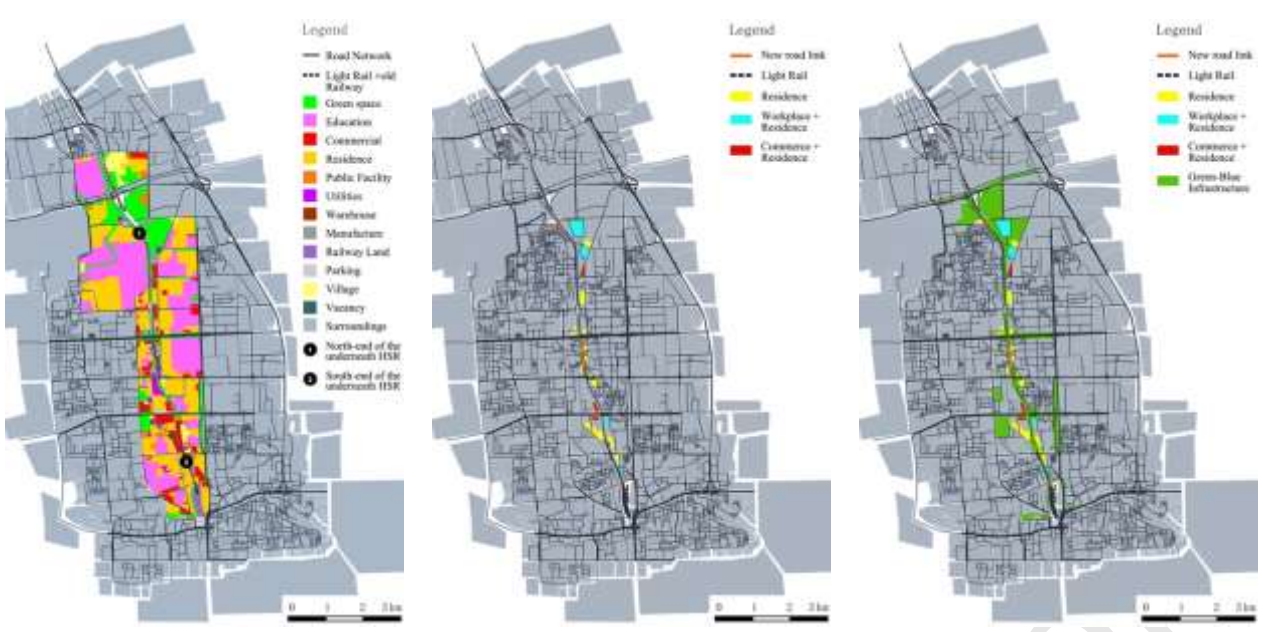

(a) **(b)** **(c)**

Figure 5. Road and land-use layout and the planned underneath part of the Jing-Zhang HSR: (a) Baseline scenario, (b) System-Internal Integration Plan0, and (c) External Integration Plan1 and 2.

Plan 0 focuses on integration within the transport and spaces system by connecting existing road networks and reusing leftover urban spaces. According to the official transportation plan, the road network above the underground section of the HSR will keep unchanged but will add some joint passages to increase accessibility. As for the above-ground parts of the HSR, underpasses (represented as orange lines in Fig. 5(a)) are used to connect the road networks on both sides. Following the planning strategies of mixed land-use and compact urban development (listed in the *Introduction*), underutilized linear spaces along the line are repurposed as residential, industrial, and commercial land-uses. Since no governmental plan describes how the vacated urban spaces will be redesigned as public open spaces after demolishing the old rail, this scheme assumes them as a linear space covered by light gray granite pavement without vegetation, which is created as a reference plan.

Based on Plan 0, Plan 1 and 2 (see Fig. 5(c)) adopt the other design methods outlined in the *Introduction* that integrates the transport and spaces system with the external ecosystem, i.e., to provide green and blue infrastructure and to reduce mobile emissions. The approaches applied in Plan 1 are transforming the old railway into a lawn and planting bushes along the main road. Plan 2 introduces a systematic blue-green approach that unifies the existing green and blue spaces into a

linear park. This scenario attempts to take the transport and spaces environment and the natural environment as a whole.

3.3. Mesoscale Pollution Estimation

After running the ABM for 24 hours under the four scenarios, it outputs the hourly numbers of cars traveling over the road network which are used as inputs to the COPERT. Although the COPERT methodology is developed based on European data, it has been applied to China in recent decades (e.g., Cai & Xie, 2007; Wang et al., 2010). Lang et al. (2012) used the measured emission factors e^h for cars with emission standards from Euro 0 to 4 to calibrate the COPERT e^h, showing that the software is suitable for assessing car emissions in Beijing. Referring to the Beijing Vehicle Activity Study (Huan et al., 2005), we assume the type of modeled vehicle as 90% passenger cars and 10% light-duty vehicles, most of which consume unleaded gasoline fuel and subject to the China IV and 5 Emission Standards (equivalent to Euro 4 and 5 standard). The mean e^h used for each type of vehicles are selected from (EEA, 2016) as shown in Supplementary Data (Table S2).

3.4. Microclimate Simulation

3.4.1. Research Sites

Based on the four mesoscale planning scenarios, we then zoom into the microscale to test the effect of transport and spaces designs on the pedestrian level environment.

Initially, at Site 1 (see Fig. 6 (a)), we conduct a comparison of experimental measurements with ENVI-met model outputs in order to validate the CFD simulation performed by ENVI-met. The parameters investigated include air temperature and relative humidity. Monitoring data was gathered by the Research Center for Eco-Environmental Sciences, Chinese Academy of Sciences and measurements were performed consecutively since the year 2002 with readings taken every 1 hour at about 22.5m above ground (on the monitoring point depicted in the Figure). Once verified ENVI-met input parameters and the CFD simulation, the same configuration files and databases are then applied to simulate the different design scenarios on site 2 for the same period.

Afterward, at Site 2 (see Fig. 6 (b)), the non-motorized transport network was severely separated by the old railway, and large tracts of public spaces were leftover coupled with a serious lack of green spaces and dedicated pedestrian infrastructures. Significant efforts should be made to improve the walking environment of Site 2; therefore, we choose it as an exemplary study field for testing different integrated transport and spaces design scenarios. As shown in Figure 6(b), three locations within this site are selected for examination of microclimate modeling outputs during the whole simulation period. Location A lies in the middle of the railway, while Location B is on the southern side of the rail. Location C is on the northern side of the railway line, close to the main road. These measurement points were selected to best capture the impact of the design interventions and provide insights into how this site will be affected.

(a) **(b)**

Figure 6. The microscale research sites: (a) Site 1 (validation site) and the monitoring point, (b) Site 2 with the locations of point A, B, and C that chosen to analyze the impact on the whole site.

3.4.2. ENVI-met Initialization

ENVI-met is formed by three parts: 1) an area input file that describes the three-dimensional geometry of the research site, 2) a configuration file that illustrates the initialization conditions such as meteorological data, and 3) databases that define sources (e.g., traffic emissions are described as linear sources), plants (include simple plants and 3D vegetation), soil, etc.

3.4.2.1. *Area Input File.* In order to represent the layout of buildings, roads, the old rail, public spaces, and vegetation precisely, we synthesize high-resolution OpenStreetMap and Baidu Maps images with

comparing with field measurements to create the area input files. Two computational files cover a vertical height of 200m with a uniform Cartesian grid.

3.4.2.2. *Configuration Wizard.* Beijing has a monsoon-influenced humid continental climate that features hot and humid summers along with cold and windy winters. To depict the atmospheric conditions, we use a historical dataset (The Weather Channel), which records the hourly values of air temperature, wind speed, wind direction, and relative humidity in Beijing since 1930. As for simulation days selection, we choose the typical days with extreme weather in the past three years when people feel the most uncomfortable in doing outdoor activities.

Primarily, to examine the impacts of design schemes on local air pollution and wind field, we conduct simulations in wintertime, a period with high NOx pollution and strong wind (Chen et al., 2015; The Weather Channel). Though spring witnesses the strongest wind, it can also dissipate the air pollutants emitted by cars and eminently improve atmospheric condition; thus, spring is not capable of representing the bad weather in Beijing. The wintertime simulations are carried out on five consecutive workdays from October 30 to November 3, 2017. The reliability of input data (pollution sources) is the main reason for chosen these days. The emission sources used for ENVI-met is derived from the traffic volume results, which were calibrated by the measured data of the typical weekdays from September to November in 2017. In addition, every year from mid-November, the government starts coal-heating after which mobile sources are not the dominant emission source in the city. Therefore, this five-day simulation can eliminate the impact of coal-fired power plants emissions.

Furthermore, to assess air temperature and thermal comfort, we simulate a period characterized by high temperature and solar radiation. According to historical data, the hottest and the most humid days in Beijing appear in the mid-July. Thus, five consecutive workdays from July 17 to 21 are picked. In ENVI-met, a typical time frame is 24—48h, so we combined three simulations for wintertime simulations and three others for summertime. Each simulation starts from 0:00, and the first two hours are not counted in the final result (see details in Supplementary Data, Table S3, S4).

3.4.2.3. *User-Defined Databases.* In the winter day simulations, a user-defined emission source input file is also needed. In this file, each road segment has a unique ID along with a designated source type. In this work, road portions are defined as line sources while road crossings as area sources and the height of release are defined at 0.5m. Samples for two kinds of source data are listed in Supplementary Data (Table S5).

3.5. Thermal Comfort Assessment

The simulated climate data from ENVI-met, i.e., air temperature, relative humidity, solar radiation, and wind speed, are imported into Bio-met and RayMan. The body parameters required for the PMV and UTCI measurement are derived from a report of the National Health Commission of China (2015). As an example, this study chooses an average Chinese man in age 35 to examine his thermal satisfaction when walking in a hot and humid summer day (July 17, 2017). The clothing insulation parameters and metabolic rate chose from (Auliciems & Szokolay, 2007) are listed in the Supplementary Data (Table S6).

3.6. Microscale Urban Design Scenarios

According to the current transport and spaces system conditions, we developed three microlevel integrated design scenarios, as presented in Figure 7. The species and features of trees, grasses, and hedges adopted in the simulation correspond to the findings of a field survey (for details Supplementary Data-Table S7).

- System-Internal Integration scenario (Plan 0): uses the remaining urban areas as residential and industrial lands, sews the dead-end roads on two sides of the railway with providing walking and cycling lanes, and replaces the old rail by a granite pavement;
- External Integration scenario (Plan 1): based upon Plan 0, supplants the granite cover by a linear grassland and adds bushes along the north main road for reducing mobile emissions;
- External Integration scenario using a blue-green approach (Plan 2): based upon Plan 1, configures a linear park equipped with a variety of trees and ponds and doubles the roadside trees.

(a) **(b)** **(c)**

Figure 7. Microscale integrated design scenarios: (a) Plan 0, (b) Plan 1, and (c) Plan 2.

4. Simulation Results

4.1. ABM Output and Model Validation

The shortest-path (initial Smart-City Model) and the quickest-path model (adjusted model) run separately for 24 hours in a workday. A comparison between the two simulations can be made based on Figure 8 and Figure 9.

Figure 8. Mean hourly traffic volume generated by the ABM using the shortest-path algorithm.

Figure 9. Mean hourly traffic volume generated by the ABM the quickest-path algorithm.

The heatmaps visualize average hourly use of each road, reflecting traffic distribution over the transport network. The road system presented in Figure 4 indicates that the most massive traffic should occur in the six highways and expressways. Hence, the model based on the quickest route algorithm is a better representative of road usage than that based on the shortest route. Vehicles moving with the shortest-path tend to choose some shortcuts (e.g., the red lines at the bottom middle of Fig. 8) which in many cases do not match the real situation.

Figure 10 gives us more insights into these road use patterns since it measures the frequency with which eight main roads are used. Two histograms show average hourly road usage of the shortest-path simulation, the real-life case, and the quickest-path simulation, during morning rush hour (6:00 am-10:00 am) and evening rush hour (3:00 pm-7:00 pm). Histogram of the shortest-path model differs widely from the real data while the quickest-path model shows more similarity with the real-life case.

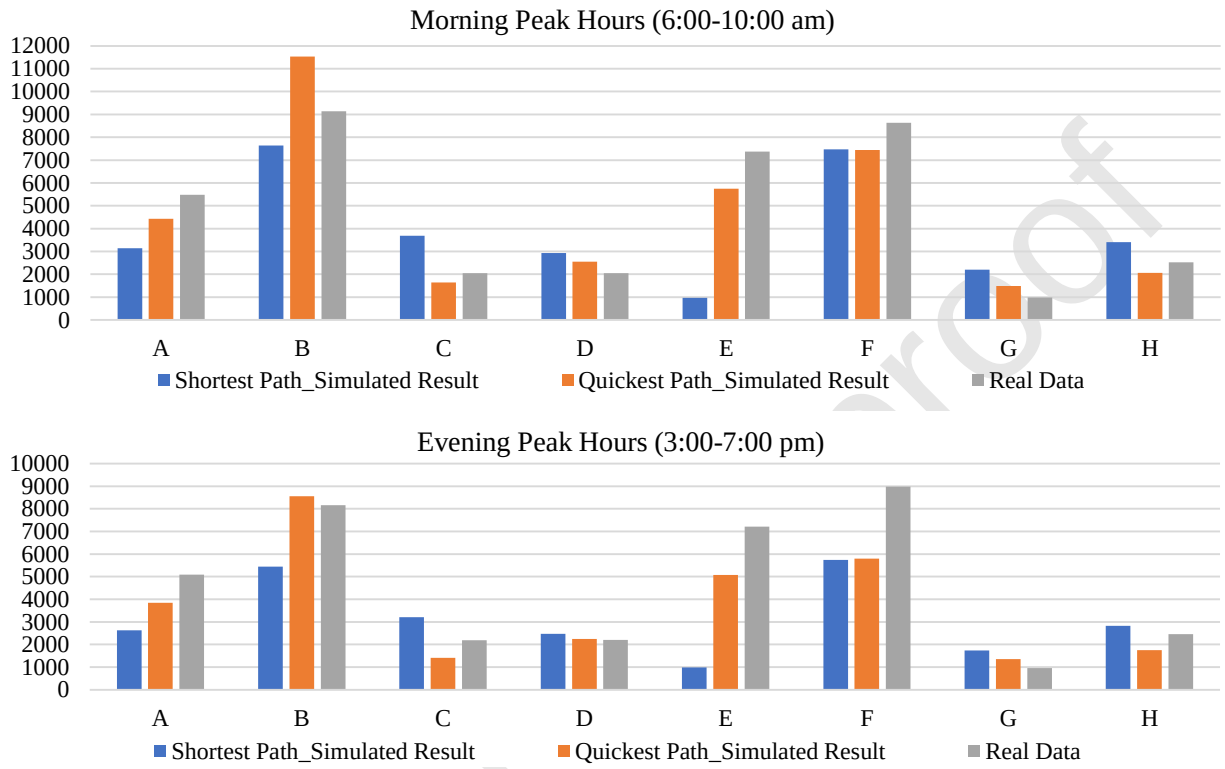

Figure 10. Histogram of morning and evening peak hours road usage of simulation using the shortest-path algorithm, real data, and simulation using the quickest-path algorithm.

Moreover, as it is shown in Table 1, Relative Error of the outputs derived from the quickest route model ranges between -30% and 50%, much smaller than those yielded by the shortest route model, ranging from -90% to 110%. Given the above, the adjusted model provides a relatively better prediction of real-world road transport.

Table 1. Relative Error (%) of the Simulated Results (positions of the road section are shown in Fig. 4).

Road sections	A	B	C	D	E	F	G	H
Shortest-path	-45.40	-24.44	62.46	27.01	-86.60	-24.92	103.25	25.15
Quickest-path	-21.76	16.10	-28.41	12.71	-25.87	-24.86	46.80	-23.45

4.2. Mesoscale Pollution Estimation

As an illustration, Figure 11 shows grams of NOx emitted by private cars averaged over a run for 24 hours. At the mesoscale, Plan 0 differs slightly from the status quo and is similar to Plan 1 and 2. In comparison with the base case, there are three significant changes in the new plans. Firstly, on the right-side highway, the sections close to the downtown pollute more NOx, peaking at more than 10kg for each hour. Secondly, the road highlighted by circle 1 in Fig. 11(b) generates nearly four times pollutants than the Baseline scenario. This is because we increased the road connectivity in this area. Finally, the road highlighted by circle 2 in Fig. 11(b) shows a slight difference to the Baseline with yielding roughly twice the amount of emissions.

(a) **(b)**

Figure 11. Mean hourly NOx pollution [g] generated in: (a) Baseline scenario and (b) Plan 0/1/2.

4.3. Microscale Climate Simulation and Model Validation

4.3.1. Model Validation on Site 1

To validate the microclimate simulations, we extract the hourly-based air temperature and relative humidity meteorological parameters from experimental measurement database during both wintertime and summertime simulation periods (from October 30 to November 3, 2017, and from July 17 to 21, 2017). The ENVI-met simulation outputs (22.5m above ground) at the monitoring point in Site 1 are compared with the real data using Relative Error as a measure.

Figure 12 shows the simulated results and measured values of air temperature in winter and summertime periods. On the whole, the simulated outputs have an overall concordance with real data during the ten simulation days. The relative error obtained by wintertime simulation is between -40% and 80%. It can be found that the model predicts lower air temperature during most of the daytime in winter. Summertime simulations generate more accurate results, the relative errors of which range from -10% to 45%.

Figure 13 compares the relative humidity values yielded by the simulation and measurements. Simulated values of the microclimate model are comparable to monitored data. In winter, the model tends to estimate higher levels of humidity with an average relative error of 67%. In summer, the model gives an excellent estimate with a mean relative error of 12%.

It can be seen that field measurement and results from ENVI-met numerical simulations, especially from the summertime simulation, are in good agreement.

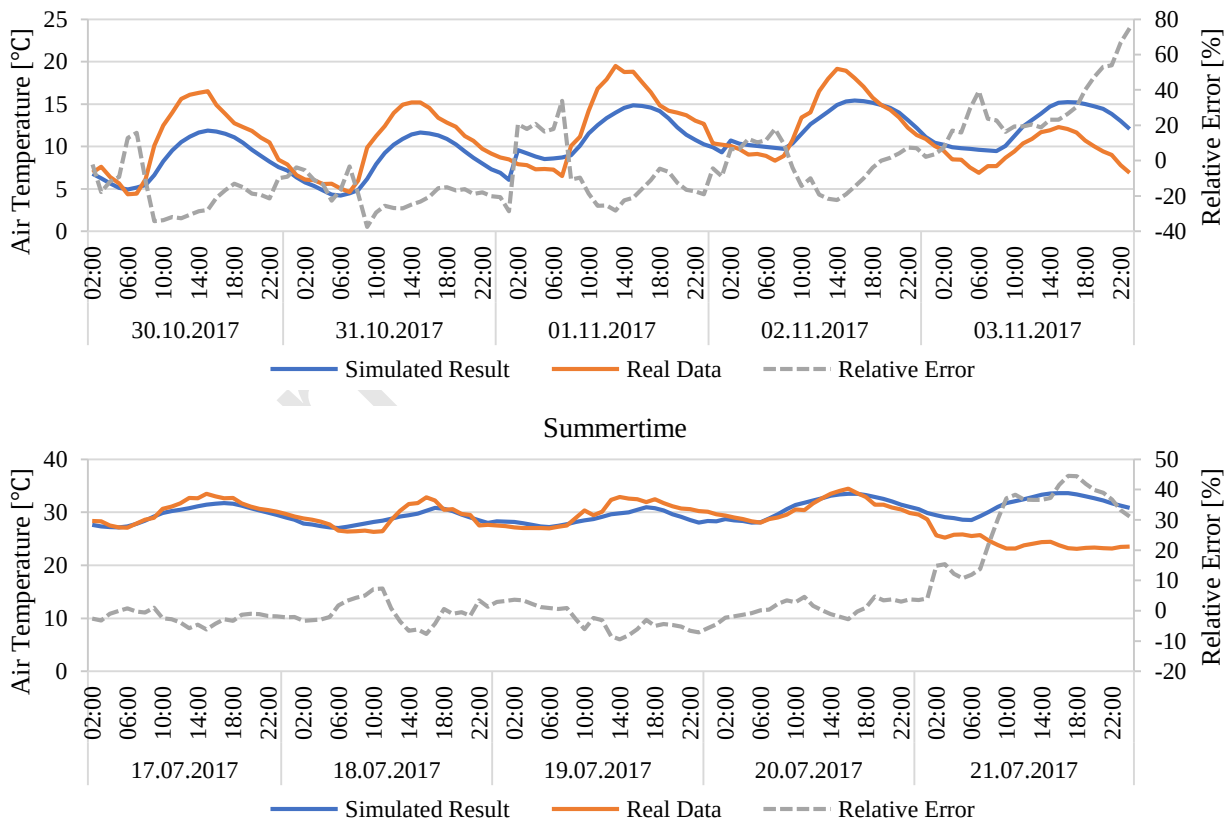

Figure 12. Simulated air temperature and real data at the monitoring point (22.5m height from the ground) and the relative error in wintertime (Oct 30—Nov 3) and summertime (July 17—21).

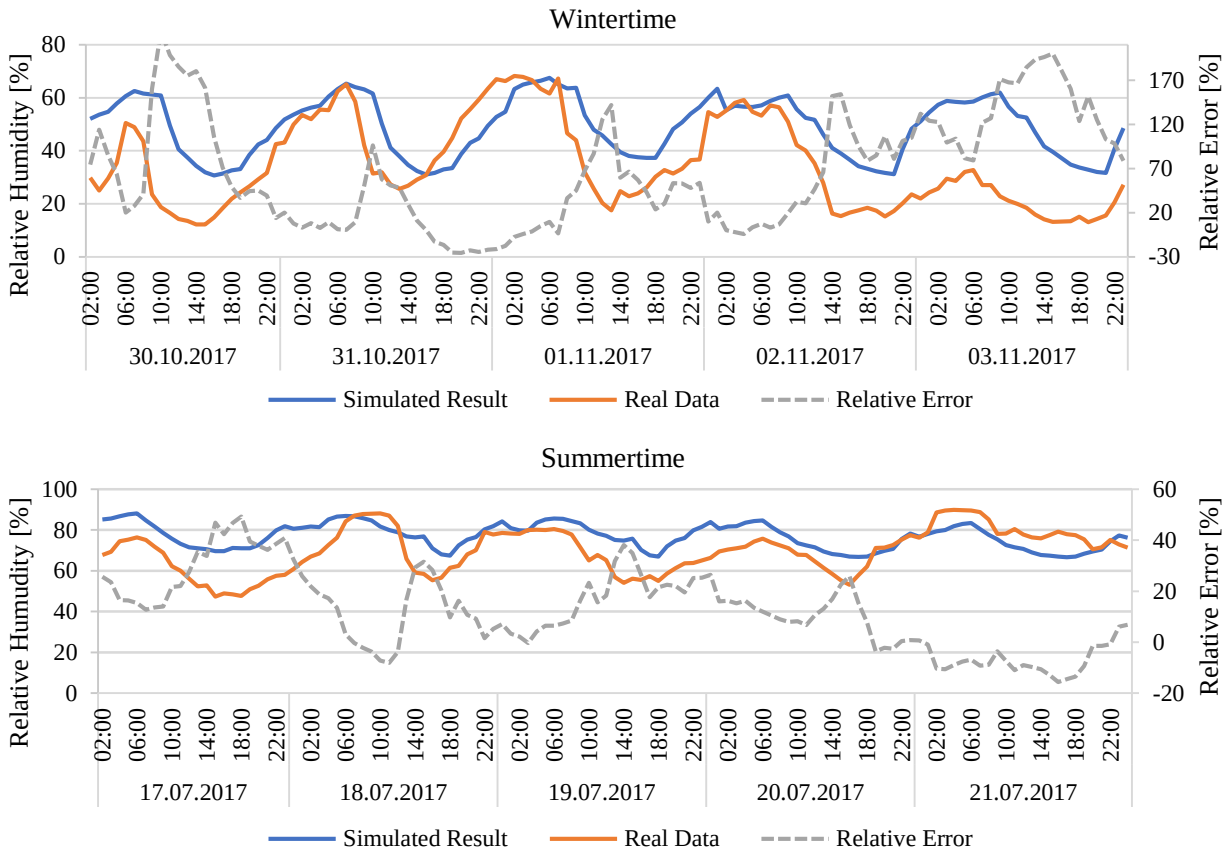

Figure 13. Simulated and observed relative humidity at the monitoring point (22.5m height from the ground) and the relative error in wintertime (Oct 30—Nov 3) and summertime (July 17—21).

4.3.2. Microclimate Simulation Results on Site 2

To start, we first use Leonardo to visualize the outputs at 13:00 (1.5m above ground) on November 2 and July 17 (examples of winter and summer simulations) for investigating the overall climatic conditions on Site 2 under the base case and Plan 0. 13:00 is the time when citizens in Beijing are likely to perform outdoor activities in all seasons. In order to present the extent to which three plans vary from the base case, we employ different analysis approaches. For example, figures depicting the absolute difference between Plan 0 and Plan 1/2 are provided for the analysis of NOx concentration and wind speed in wintertime.

4.3.2.1. *Pollution Concentration in Wintertime.* As depicted in Figure 14(a), NOx concentration of the base case is in-between 0—0.0766mg/m^3 at 13:00 with the peak pollution appearing at a road crossing. Figure 14(b) shows the distribution of NOx pollution of Plan 0, in which more particles were generated from the upper left-hand corner (northwest) than in the base case, peaking at 0.0940mg/m^3. Correspondingly, the polluted range of the linear open space in the middle (position

of the old railway) shrinks closer to the main road. This probably because after reconfiguring the road network and land-uses, the north-south secondary road (encircled by circle 2 in Fig. 11(b)) on the left side of the sampling area was used intensively while car trips through the linear open space decreased.

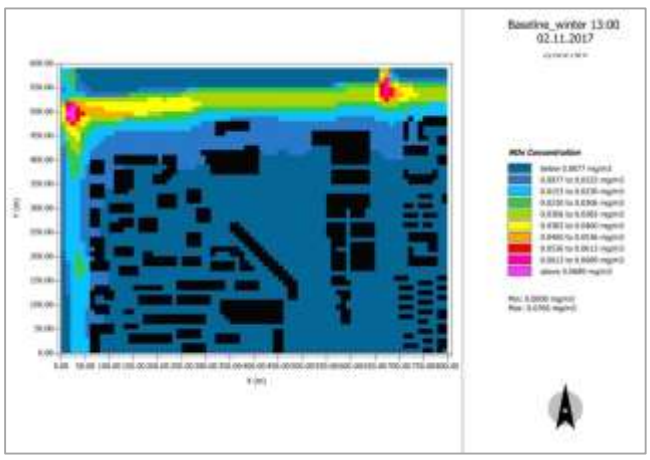

(a)

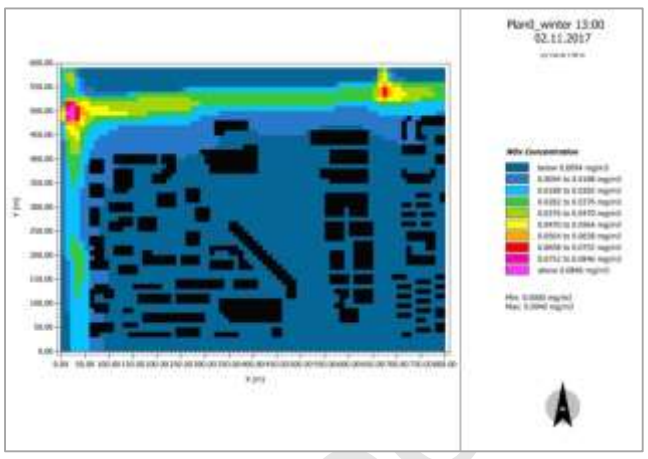

(b)

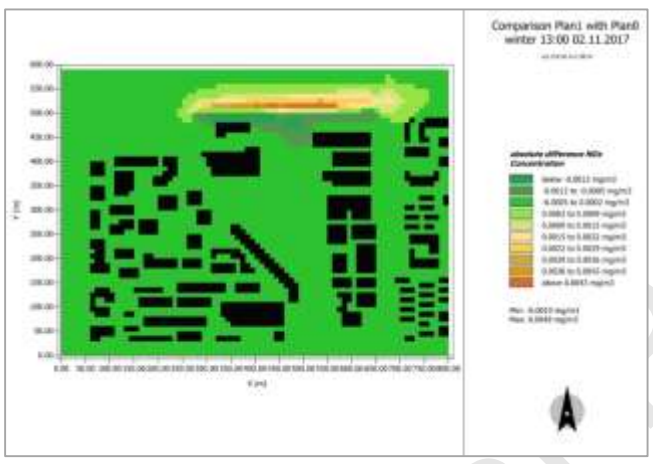

(c)

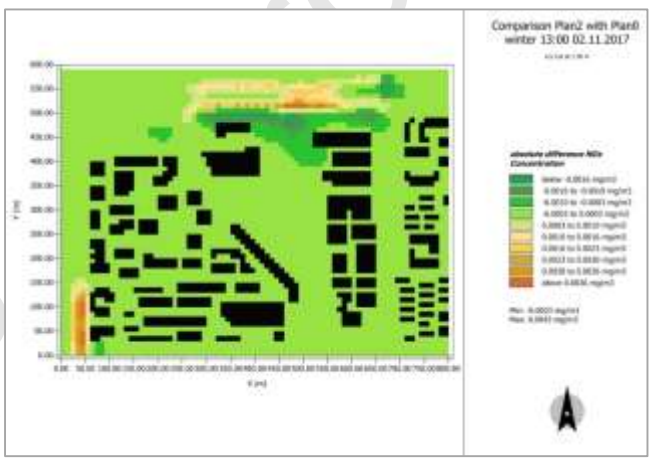

(d)

Figure 14. NOx concentration [mg/m^3]: (a) in Baseline scenario, (b) in Plan 0. NOx concentration [mg/m^3] comparison between: (c) Plan 1 and Plan 0, and (d) Plan 2 and Plan 0.

Comparing to Plan 0, Plan 1 (Fig. 14(c)) shows a lower-level of NOx concentration (decrease by 1.9µg/m^3) on the upper of the linear grassland. This demonstrates the influence of the bushes planted along the main road in dispersing and depositing particles come from the upper left corner. At the same place on the linear open space, Plan 2 (Fig. 14(d)) displays a distinct difference to Plan 0, showing a decrease of 2.3µg/m^3. This reveals that the configuration of doubled road trees with roadside bushes substantially improves the air quality in downwind areas. The bushes employed along the secondary road (on the lower left corner) is proved to have a similar impact on decreasing the downwind area NOx pollution.

4.3.2.2. *Wind Speed in Wintertime.* Figure 15 (a) and (b) show that changing the lands of the right side of the railway into high-rise residential and industrial buildings leads to a wind speed rise by 0.2m/s at the south end of the linear open space where tall buildings have been added. An addition of grasses and bushes along the main road in Plan 1 reduces wind speed by 0.76m/s for the near-road open areas in comparison with Plan 0 (see Fig. 15(c)). By deploying a forest and ponds on the linear park, Plan 2 contributes substantially to wind velocity decrease for the near-road places and the park itself with a maximum reduction of 0.85m/s (Fig. 15(d)).

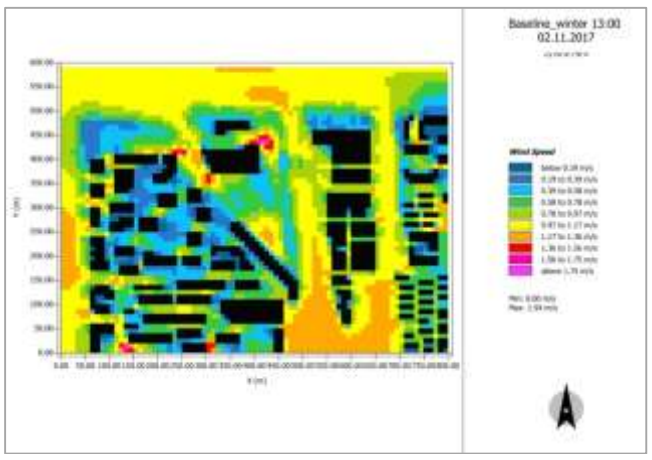

(a)

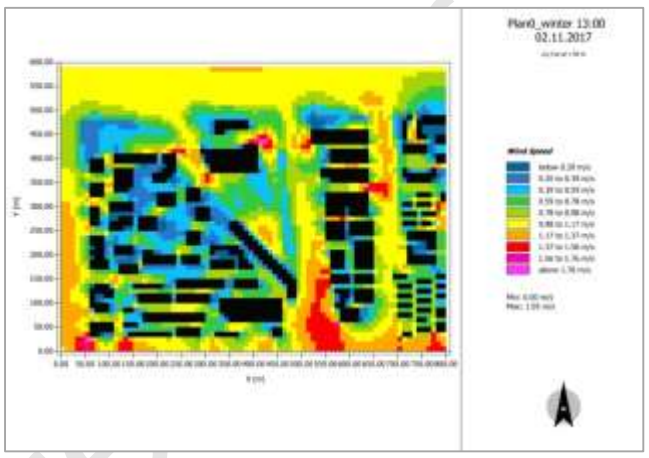

(b)

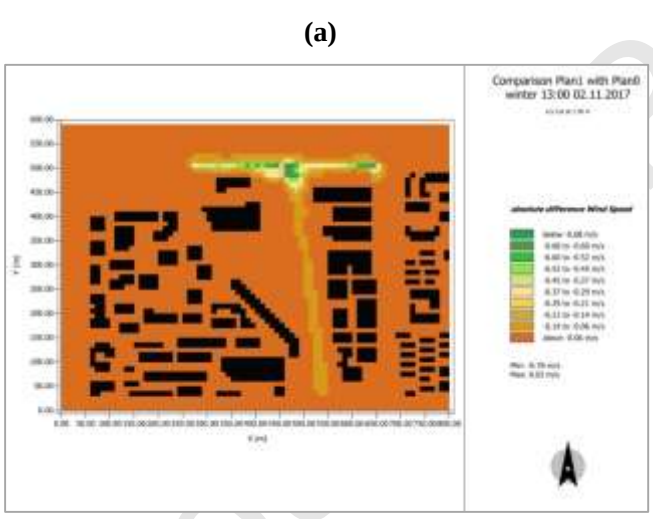

(c)

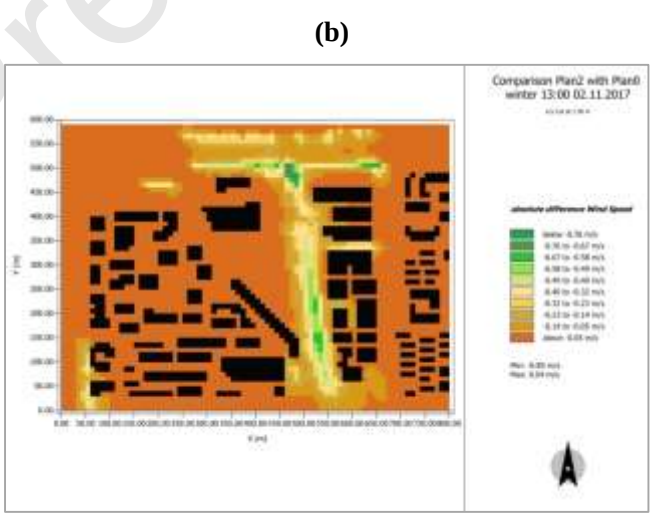

(d)

Figure 15. Wind speed [m/s]: (a) in Baseline scenario and (b) in Plan 0.
Wind speed [m/s] comparison between: (c) Plan 1 and Plan 0, and (d) Plan 2 and Plan 0.

Comparing the Baseline scenario outputs generated on the selected locations shows that point C has the lowest wind speed during most of the simulation time (depicted in Fig. 16). Point A and B that lies in the middle and southern side of the railway area experience stronger wind. Plan 0 triggers wind speed increases at all locations while Plan 1 reduces wind speeds to a similar level of Baseline.

At location A and B, it is eminent that Plan 2 can significantly reduce wind velocity with an average reduction of 0.2m/s in comparison with the base case.

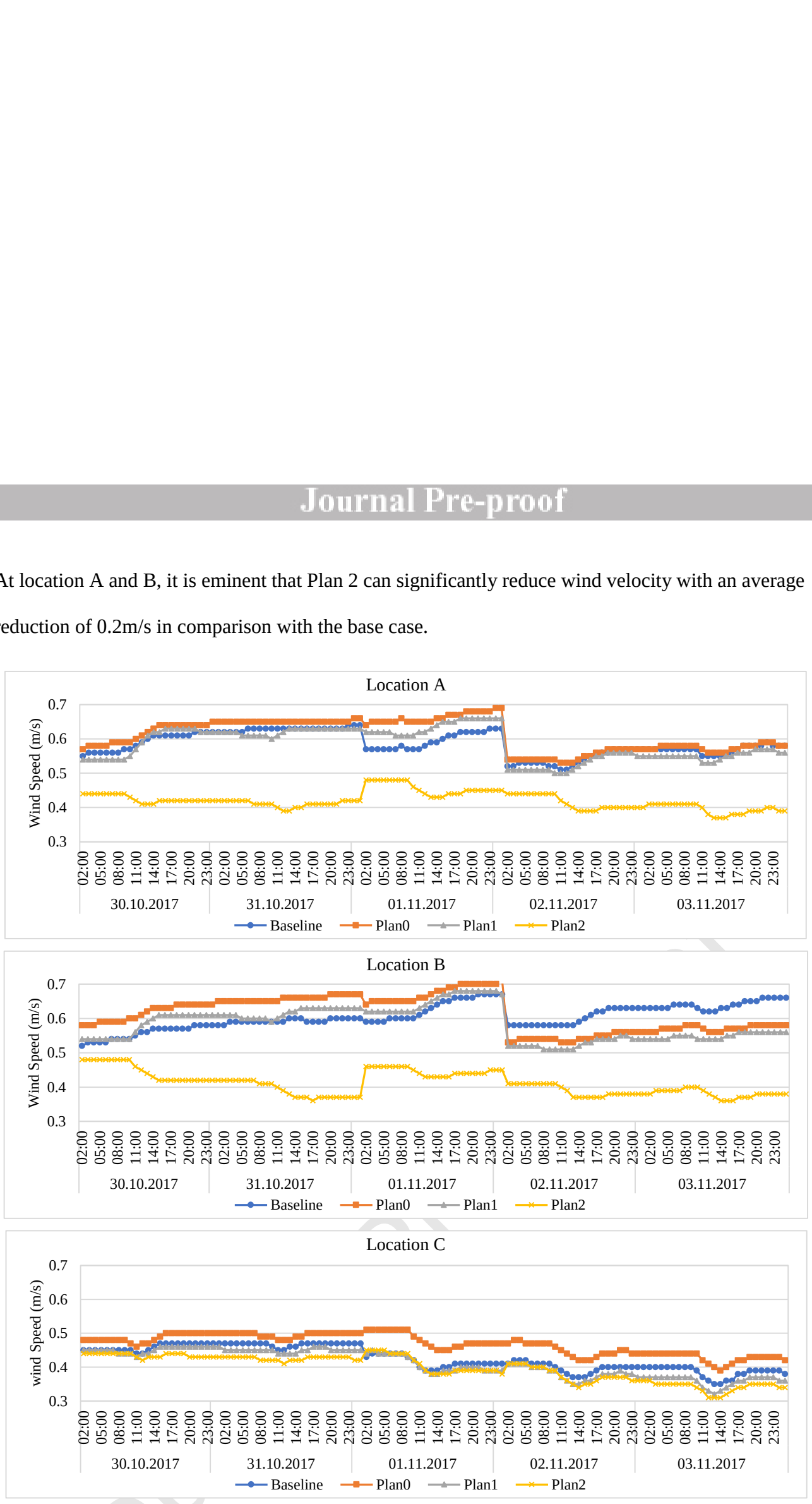

Figure 16. Hourly wind speed [m/s] for the summertime simulation days (Oct 10 – Nov 03, 2017) at location A, B, and C (1.5m height) under four scenarios.

4.3.2.3. *Air Temperature in Summertime.* It can be seen from Figure 17 (a) that the temperature on main roads (peaking at 32.76°C) is higher than the railway surroundings (in-between 30.78—31.11°C) in the base case. In Plan 0, the temperature of the railway surroundings is lowered to 30.02—30.35°C, as shown in Figure 17(b).

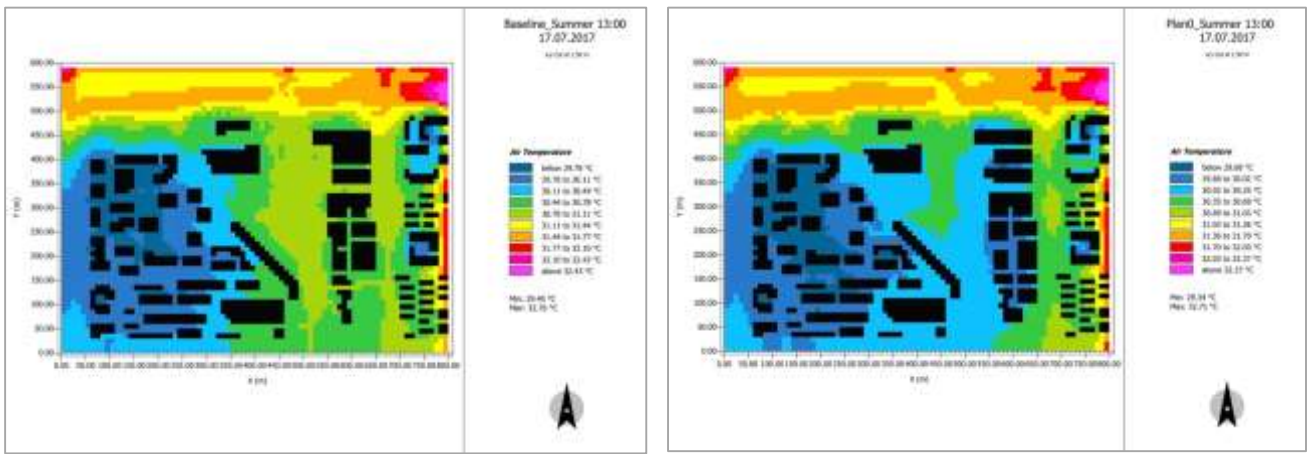

(a) **(b)**

Figure 17. Air temperature [°C] in (a) Baseline scenario and (b) plan0. Positions of location A, B, and C.

An analysis of air temperature variations during the five simulation days at exemplary locations are summarized in Figure 18. In general, the overall temperature at Location C (in roadside open space) is lower than Location A and B (in the linear railway area). It can be found that removing the old rail and covering natural soil with materials in Plan 0 lead to a reduction in ambient air temperature in most days. In particular, the maximum difference between Baseline and Plan 0 is up to 0.7°C, occurred at Location A on July 19. The impact of Plan 1 (replacing granite material with grass) and Plan 0 on heat stress mitigation is similar. Plan 2, which introduces a blue-green approach, proved to be the most effective scheme to lower air temperature consistently, especially at Location A and B (on the linear park). An addition of ponds, roadside trees, forest, and grass contributes to a decrease of temperature by roughly 1°C at 15:00 on July 20 and 21 compared to the status quo.

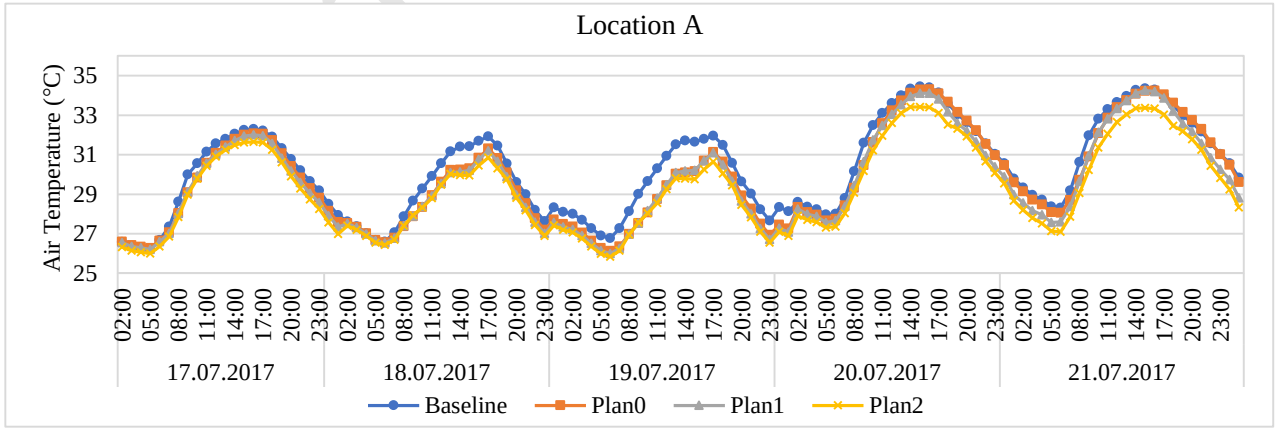

Figure 18. Hourly mean air temperature for the summertime simulation days (Oct 10 – Nov 03, 2017) at Location A, B, and C (1.5m height) under four scenarios.

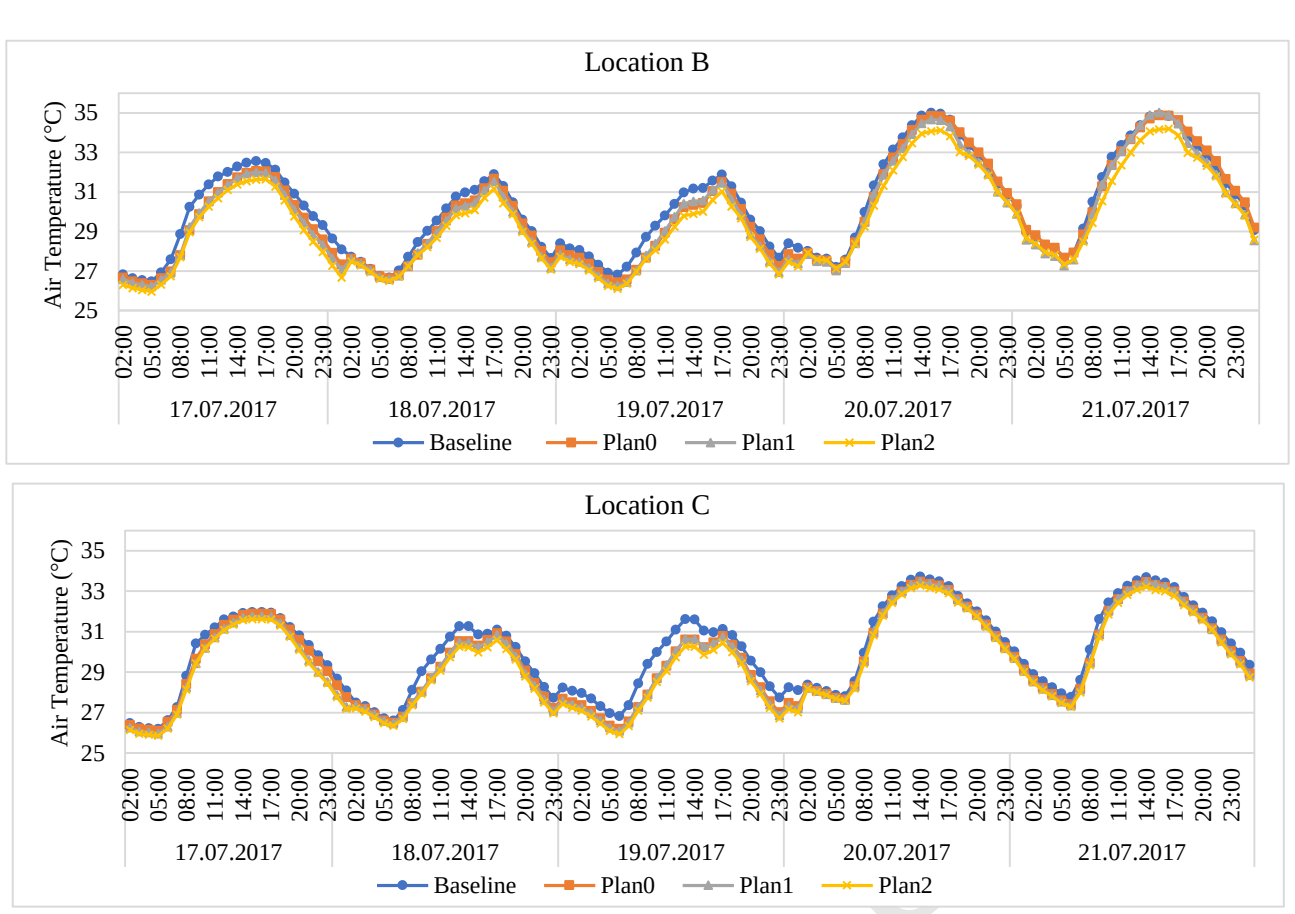

Figure 18. Hourly mean air temperature for the summertime simulation days (Oct 10 – Nov 03, 2017) at Location A, B, and C (1.5m height) under four scenarios.

4.3.2.4. *Predicted Mean Vote (PMV) in Summertime.* Building upon the previous results, we then evaluate the outdoor thermal comfort through the PMV index. First of all, the PMV of the different scenarios at 13:00 is compared. Changing the old rail to a granite covered open space slightly promotes the thermal comfort of Plan 0 in which more areas have a PMV of under 5 (see Fig. 19 (a) and (b)). By comparing Plan 1 and 0, it can be concluded that provision of the linear grassland and hedges along the main road contributes to a substantial decrease in PMV (Fig. 19(c)). The blue-green infrastructure designed in Plan 2 has the most considerable impact; it enhances the overall thermal comfort of the linear park, where the PMV of most patches are below 4 (Fig. 19(d)).

4.3.2.5. *Universal Thermal Climate Index (UTCI) in Summertime.* The final part of this research assesses the outdoor thermal comfort through UTCI. Subsequently, the UTCI at Location A—C is investigated to explore the duration and degree of thermal stress in the four scenarios. As shown in Figure 20, the thermal comfort variations between four plans are eminent at Location A and B. On these two points, three plan alternatives all contribute to a decrease in UTCI values during the daytime

(6:00—17:00). Plan 0 largely reduces the UTCI temperature from 6:00—9:00, after which the reduction seems to be minimal.

From 9:00 to 17:00 on every simulation day, individuals experience severe heat conditions in all scenarios. Comparing to Baseline, Plan 1 improves the daytime thermal sensation noticeably, decreasing UTCI by nearly 2°C, while Plan 2 decreases the value even more (reduces 6.5°C at 9:00 on July 17). Plan 2 provides the best thermal condition for individuals that the very strong heat stress appeared on July 17—19 along with the extreme heat stress (more than 46°C) in the following days have been mitigated. In the morning (2:00—6:00), Plan 2 slightly increases UTCI by almost 1°C which may be caused by the increase of relative humidity due to higher coverage of vegetation (Wong & Peck, 2005). At Location C, however, there is no apparent difference between the four scenarios, despite a UTCI decrease at 9:00 in Plan 0,1,2 (roughly 5°C).

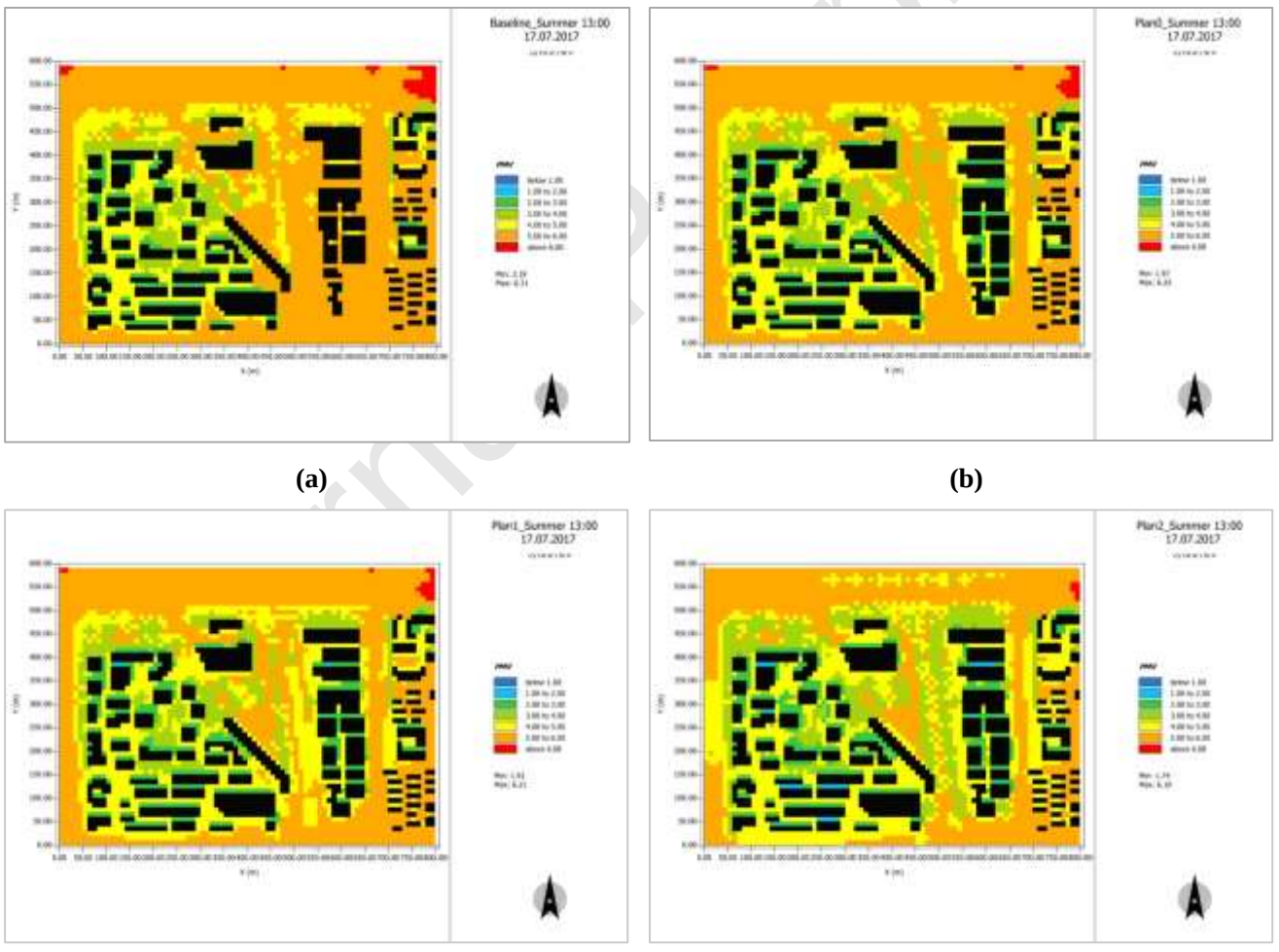

(a) **(b)**

(c) **(d)**

Figure 19. PMV in: (a) Baseline scenario, (b) Plan 0, (c) Plan 1, and (d) Plan 2.

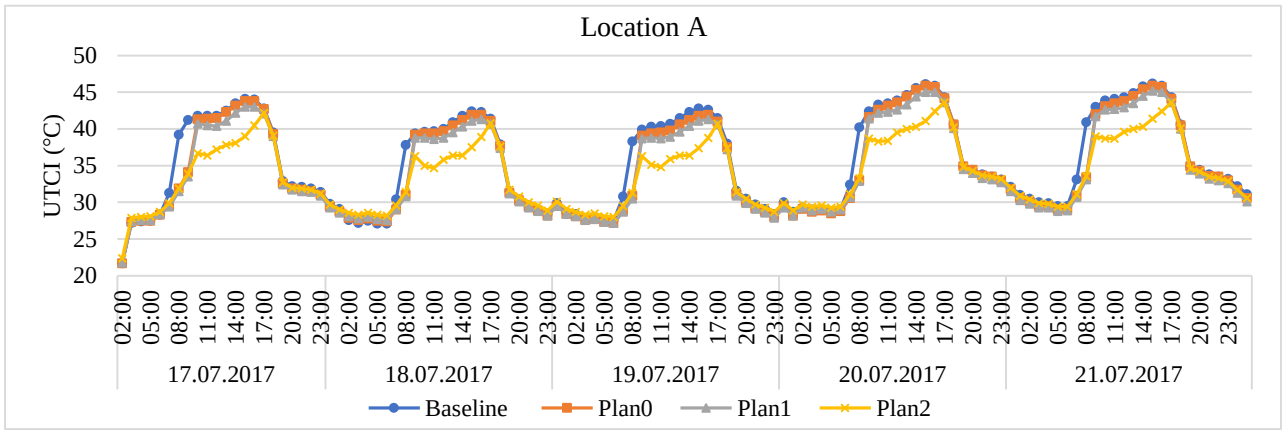

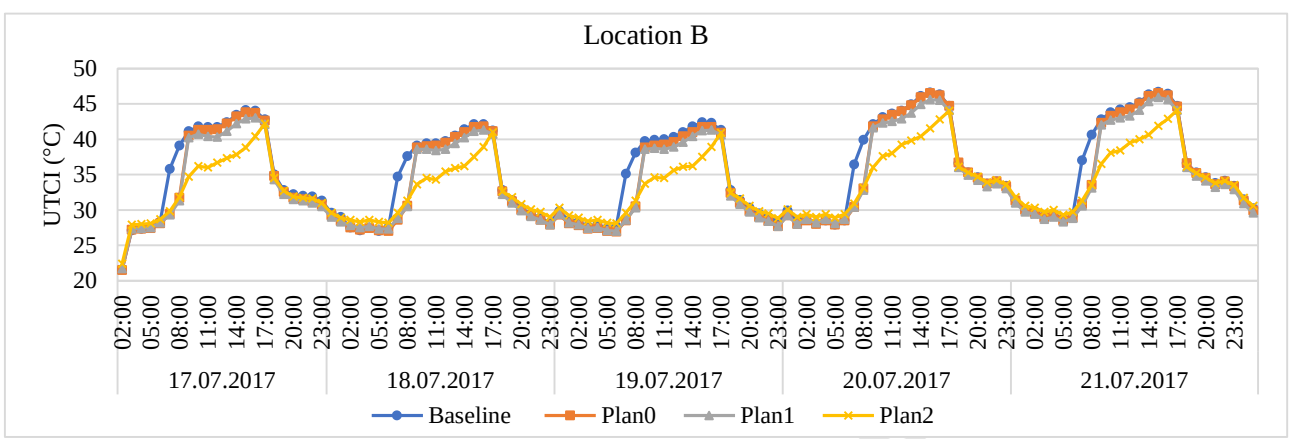

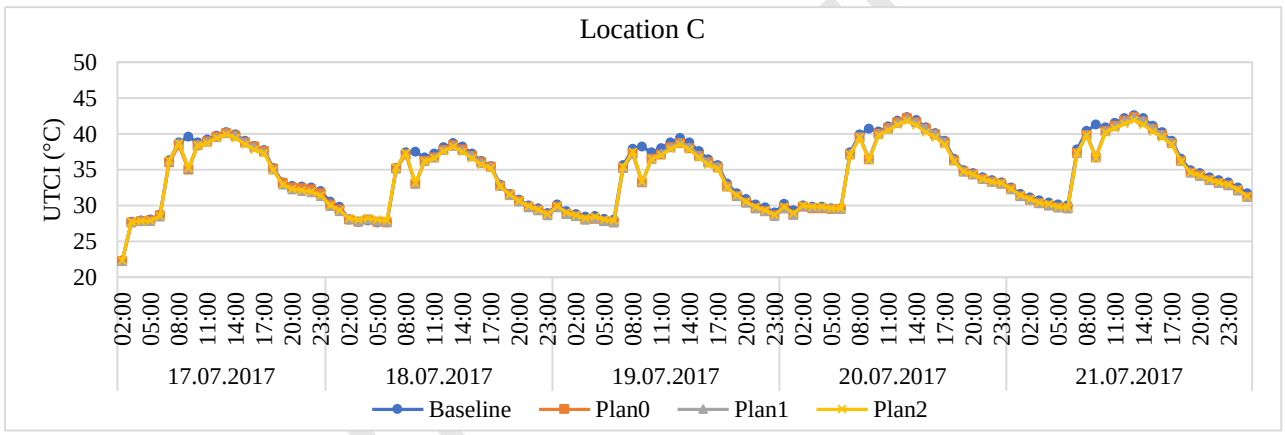

Figure 20. Hourly UTCI for the summertime simulation days (Oct 10 – Nov 03, 2017) at Location A, B, and C (1.5m height) under four scenarios.

5. Discussions and Conclusion

In a context of climate change, the effects of air pollution and UHI can be broadly intensified in large cities. The conventional urbanization process of prioritizing motorized transport infrastructure development should consider the challenge of planning integrated transport infrastructure and public space systems, characterized by pedestrian-friendly and climate-sensitive. This paper examines the impacts of using different design strategies in a Beijing case study through the lens of mesoscale traffic-related NOx emissions, and microscale NOx concentrations and wind velocity in winter along

with air temperature in summer. Human scale thermal comfort is assessed via PMV and UTCI indices. The multiscale simulation can be of the paramount value for transport and spaces systems planning.

Initial results demonstrate that changes in the road network, land-use, and public space arrangement at a meso/urban scale have a direct impact on vehicle trip generation, resulting in changes in traffic emission distributions, though the baseline NOx emission quantity needs to be validated in future work for supporting final decision-making. The traffic-deduced air pollutant concentration under micro/block scale scenarios differ eminently.

This study shows that a System-Internal Integration Plan (0) which applies the strategies of mixed land-use, compact urban development, connected road network equipped with dedicated walking and cycling infrastructures is insufficiently helpful for improving local air quality and pedestrian comfort. In certain areas, air quality may be even worsened due to the heavier traffic on adjacent roads. The compact development accompanied by high-rise buildings will increase the wind speed of particular open spaces around tall buildings by 0.2m/s.

An External Integration scenario (Plan 1) that applies both the aforementioned strategies and the green infrastructure approach is a feasible means for reducing traffic emissions and promoting the outdoor atmospheric environment and human's thermal satisfaction. Given that the emission sources input to the microscale Plans (0, 1, 2) differ marginally, it could be concluded that provisions of green infrastructures such as vegetation barriers can mitigate road traffic emissions by increasing particle dispersion and deposition. Some research shows that vegetation barriers can be useful for pollution abatement only if they are appropriately positioned and configured (Morakinyo & Lam, 2016; Wania et al., 2012). In this respect, this scenario configures near-road hedges at the height of 2m, which prove effective for reducing NOx concentration in downwind open areas by a maximum of 1.9μg/m^3, in comparison with Plan 0. However, pollutants accumulated on the upwind side of the vegetation barrier due to the barrier effect, resulting in a maximum increase of 4.9μg/m^3 for NOx concentration.

Noteworthy, an External Integration scenario using a holistic strategy that concentrates on both integrated design within the transport infrastructure and public space system and mitigating the

system externalities (e.g., air pollution) by introducing a blue-green approach (e.g., linear parks) is the most effective way for achieving an environmentally- and pedestrian- friendly transport and spaces design. As presented in Plan 2, increasing the number of road trees and roadside hedges can lessen the downwind area NOx concentration in Plan 0 by nearly 2.3μg/m^3. The level declines with increasing the distance from the main road. It is worth noting that the trees used in this case feature wide and low porosity in order to guarantee the pollutant dispersion effects since in some cases trees may contribute to air quality deterioration (Abhijith et al., 2017).

Furthermore, the holistic approach has advantages in reducing the airflow in winter and the high temperature in summer, leading to a speed decrease of 0.85m/s (at 13:00) to Plan 0 ; however, a siloed green infrastructure solution such as a grassland (Plan 1) can only lead to a maximum of 0.76m/s reduction. At Location A and B, Plan 2 contributes to a decrease in air temperature by roughly 1°C (at 15:00 on July 20, 21) compared to the status quo. Moreover, pedestrians are exposed mostly to a comfortable thermal environment in Plan 2. It is clear that doubling the near-road vegetation and replacing the old rail by a linear park provides an average decrease of 1 PMV compared to the base case. Although the maximum value of PMV is above 5 when pedestrians are crossing an unshaded area, individuals could reach a thermal comfort condition when walking in the shade of trees. The blue-green approach also provides co-benefits such as raising adjacent residential land values (Zhang et al., 2012) and reducing cooling energy expenditure. Empirical studies indicate when the air temperature is higher than 26°C in summer in Beijing, every 0.5°C temperature decrease leads to a reduction of cooling energy consumption by roughly 20×10^7 W at peak hour (Zhang et al., 2011).

The thermal comfort assessment through UTCI testified that all three plan alternatives contribute to a decrease in UTCI at the linear open space (Location A and B) during the daytime. Though the reduction of Plan 0 is minimal, Plan 1 noticeably improves the daytime thermal sensation and reduces UTCI by about 2°C. Plan 2 provides the best thermal condition for individuals, decreasing the value by 6.5°C (at 9:00 on July 17), mitigating the very strong heat stress on July 17—19 and the extreme heat stress in the following days.

From the simulation results in this case study, it is clear that the multiscale modeling method can give valuable insights into the impact of urban design choices on traffic pollution and microclimate condition, allowing an iterative process of updating designs based on feedback from the computational evaluation. Though this paper was initiated with assessments of a specific urban environment in Beijing, the urban morphology and meteorology data used to drive the simulations are commonly encountered in many other cities, especially those characterized by the monsoon-influenced humid continental climate. Therefore, the proposed urban modeling-design framework for testing meso and micro scale transport infrastructure and public space design alternatives is expected to apply quite widely within the limitations of the simulation assumptions and measurement accuracy of the computational models adopted.

With the same coupling method, other traffic prediction techniques could also be employed to take advantage of mode choice models and other route planning algorithms (e.g., considering congestion levels). Traffic emission calculations could be extended to measure traffic-related anthropogenic heat and humidity emissions, which can then be included within microclimate simulation (Girgis et al., 2016). Moreover, the ENVI-met simulation though considers heat storage in soil/road surfaces, the transient thermal effects in other materials such as walls are not simulated (Bruse, 2004) that could be improved. Some studies also demonstrated that ENVI-met tends to overestimate near-ground air temperature during nighttime, but slightly underestimate the value during the day for near road (Yang et al., 2013). In future work, application of a more realistic soil model would be helpful for addressing this issue.

Next steps in our research are to feed the generated microclimatic conditions and thermal comfort back into the agent-based model and update the location and route choice algorithms to allow agents to consider outdoor environmental quality (shown as dash lines in Fig. 21). For example, an updated modeling tool may allow pedestrian agents to choose the high-level thermal comfort public spaces for leisure activities and the less polluted routes for their commute. Human exposure to air pollution can be studied too. Besides, the KIPs presented in Figure 2 could be chosen depending on the specific

targets of realistic planning projects. Finally, this bottom-up environmental analysis framework may lead to decision support tools embedded in the early stage of urban design processes. The integration of climatology research and applied urban design is beneficial for guiding high-level planning.

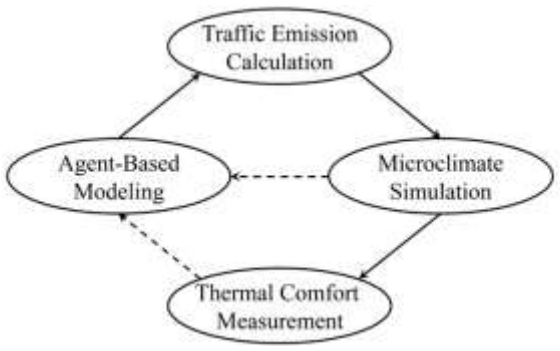

Figure 21. Future work of the coupled modeling methodology.

Acknowledgments

The research is based on a joint-PhD program between the University of Chinese Academy of Sciences (UCAS) and Imperial College London (ICL) and partially supported by a scholarship offered by the UCAS (no.158, 2016). The authors thank Dr Fei Yan (Beijing Jiaotong University, BJTU), Beijing Transport Institute, and DiDi for providing the sample of traffic data. We thank Mr Xu Sun and Dr Weiqi Zhou (Research Center for Eco-Environmental Sciences, Chinese Academy of Sciences) for sharing the monitoring meteorological data. We also thank Prof Cedo Maksimovic (ICL) for making ENVI-met software available for this research and giving insightful comments to improve the paper. The authors are grateful to Ms Ge Zhan (Re-Space Culture Development Ltd.) for sharing her previous fieldwork on the Jing-Zhang High-Speed Rail project, and Mr Lei Liu (China Railway 14th Bureau Group Co., Ltd.) for offering the official transportation plans of the High-Speed Rail project.

Declaration of Conflicting Interests

None.

References

Abhijith, K., Kumar, P., Gallagher, J., McNabola, A., Baldauf, R., Pilla, F., Broderick, B., Di Sabatino, S., & Pulvirenti, B. (2017). Air pollution abatement performances of green infrastructure in open road and built-up street canyon environments–A review. *Atmospheric environment, 162*, 71-86.

Anciaes, P. R., Boniface, S., Dhanani, A., Mindell, J. S., & Groce, N. (2016). Urban transport and community severance: Linking research and policy to link people and places. *Journal of Transport & Health, 3*(3), 268-277.

Aschwanden, G. D. (2014). *Health and Place: an analysis of the built environment's impact on walking behavior and health.* (Doctoral dissertation), ETH Zurich.

ASHRAE. (2010). *Thermal environmental conditions for human occupancy*: ASHRAE Standard 55.

Auliciems, A., & Szokolay, S. V. (2007). *Thermal comfort*.

Aultman-Hall, L., Roorda, M., & B., B. (1997). Using GIS for evaluation of neighbourhoods pedestrian accessibility. *Journal of Urban Planning and Development, 123*(1), 10-17.

Beijing Haidian Yearbook Editorial Committee. (2017, 2018.11.19). Beijing Haidian Yearbook. Retrieved from http://hdszb.bjhd.gov.cn/hdnj/njcg/2017nj/201811/t20181120_1589998.htm

Beijing Transport Insitute. (2016). *2016 Beijing Transport Annual Report*. Retrieved from Beijing, China: http://www.bjtrc.org.cn/InfoCenter/NewsAttach/2016%E5%B9%B4%E5%8C%97%E4%BA%AC%E4%BA%A4%E9%80%9A%E5%8F%91%E5%B1%95%E5%B9%B4%E6%8A%A5_20161202124122244.pdf

Beijing Transport Insitute. (2017). *2017 Beijing Transport Annual Report*. Retrieved from Beijing, China: http://www.bjtrc.org.cn/InfoCenter/NewsAttach/2017%E5%B9%B4%E6%8A%A5%E6%9C%80%E7%BB%88.pdf

Beijing Transport Insitute. (2018). *2018 Beijing Transport Annual Report*. Retrieved from Beijing, China: http://www.bjtrc.org.cn/InfoCenter/NewsAttach/2018%E5%B9%B4%E5%8C%97%E4%BA%AC%E4%BA%A4%E9%80%9A%E5%8F%91%E5%B1%95%E5%B9%B4%E6%8A%A5.pdf

Blazejczyk, K., Epstein, Y., Jendritzky, G., Staiger, H., & Tinz, B. (2012). Comparison of UTCI to selected thermal indices. *International Journal of Biometeorology, 56*(3), 515-535.

Borrego, C., Tchepel, O., Costa, A., Amorim, J., & Miranda, A. (2003). Emission and dispersion modelling of Lisbon air quality at local scale. *Atmospheric environment, 37*(37), 5197-5205.

Bruse, M. (2002). *Multi-Agent Simulations as a tool for the assessment of urban microclimate and its effect on pedestrian behaviour*. Paper presented at the International Congress on Environmental Modelling and Software. https://scholarsarchive.byu.edu/iemssconference/2002/all/73

Bruse, M. (2004). *ENVI-met 3.0: updated model overview*. Retrieved from www.envi-met.com

Bruse, M. (2007). Particle filtering capacity of urban vegetation: A microscale numerical approach. *Berliner Geographische Arbeiten, 109*, 61-70.

Cai, H., & Xie, S. (2007). Estimation of vehicular emission inventories in China from 1980 to 2005. *Atmospheric environment, 41*(39), 8963-8979.

Carmona, M. (2003). *Public places, urban spaces: the dimensions of urban design*. Oxford: Architectural Press.

Cervero, R., Guerra, E., & Al, S. (2017). *Beyond Mobility: Planning Cities for People and Places*: Island Press.

Chatzidimitriou, A., & Yannas, S. (2016). Microclimate design for open spaces: Ranking urban design effects on pedestrian thermal comfort in summer. *Sustainable Cities and Society, 26*, 27-47.

Chen, L., & Ng, E. (2012). Outdoor thermal comfort and outdoor activities: A review of research in the past decade. *Cities*, *29*(2), 118-125.

Chen, W., Yan, L., & Zhao, H. (2015). Seasonal variations of atmospheric pollution and air quality in Beijing. *Atmosphere*, *6*(11), 1753-1770.

Chokhachian, A., Santucci, D., & Auer, T. (2017). A Human-Centered Approach to Enhance Urban Resilience, Implications and Application to Improve Outdoor Comfort in Dense Urban Spaces. *Buildings*, *7*(4), 113.

Congress for the New Urbanism. (2000). Charter of the New Urbanism. *Bulletin of Science, Technology & Society*, *20*(4), 339-341. doi:10.1177/027046760002000417

De Nazelle, A. (2007). *Risk assessment of a pedestrian-oriented environment.* (Doctoral dissertation), The University of North Carolina at Chapel Hill, Chapel Hill, US.

De Nazelle, A., Nieuwenhuijsen, M. J., Antó, J. M., Brauer, M., Briggs, D., Braun-Fahrlander, C., Cavill, N., Cooper, A. R., Desqueyroux, H., & Fruin, S. (2011). Improving health through policies that promote active travel: a review of evidence to support integrated health impact assessment. *Environment international*, *37*(4), 766-777.

Du, Y., & Mak, C. M. (2018). Improving pedestrian level low wind velocity environment in high-density cities: A general framework and case study. *Sustainable Cities and Society*, *42*, 314-324.

European Environment Agency. (2016). *EMEP/EEA air pollutant emission inventory guidebook 2016*. . Retrieved from Copenhagen, Denmark: https://www.eea.europa.eu/publications/emep-eea-guidebook-2016

Ewing, R., & Cervero, R. (2010). Travel and the built environment: a meta-analysis. *Journal of the American planning association*, *76*(3), 265-294.

Fanger, O. (1972). *Thermal comfort* New York, US: McGraw-Hill Book Company.

Fenger, J. (1999). Urban air quality. *Atmospheric environment*, *33*(29), 4877-4900.

Fiala, D., Lomas, K. J., & Stohrer, M. (2001). Computer prediction of humanthermoregulatory and temperature responses to a wide range ofenvironmental conditions. *International Journal of Biometeorology*, *45*, 143-159.

Geofabrik. (2017). China-latest-free. Retrieved 28/02/2018 https://download.geofabrik.de/asia/china.html

Girgis, N., Elariane, S., & Elrazik, M. A. (2016). Evaluation of heat exhausts impacts on pedestrian thermal comfort. *Sustainable Cities and Society*, *27*, 152-159.

Gkatzoflias, D., Kouridis, C., Ntziachristos, L., & Samaras, Z. (2007). *COPERT 4: Computer programme to calculate emissions from road transport*: European Environment Agency.

Hao, J., He, D., Wu, Y., Fu, L., & He, K. (2000). A study of the emission and concentration distribution of vehicular pollutants in the urban area of Beijing. *Atmospheric environment*, *34*(3), 453-465.

Hatzopoulou, M., & Miller, E. J. (2010). Linking an activity-based travel demand model with traffic emission and dispersion models: Transport's contribution to air pollution in Toronto. *Transportation Research Part D: Transport and Environment*, *15*(6), 315-325.

Havenith, G., Fiala, D., Błażejczyk, K., Richards, M., Bröde, P., Holmér, I., Rintamäki, H., Benshabat, Y., & Jendritzky, G. (2011). The UTCI-ClothingModel. . doi:10.1007/s00484-011-0451-4. *International Journal of Biometeorology*.

Heeres, N., Tillema, T., & Arts, J. (2016). Dealing with interrelatedness and fragmentation in road infrastructure planning: an analysis of integrated approaches throughout the planning process in the Netherlands. *Planning Theory & Practice*, *17*(3), 421-443.

Huan, L., Chunyu, H., Lents, J., Davis, N., Osses, M., & Nikkila, N. (2005). *Beijing vehicle activity study*. *International Sustainable Systems Research*. Retrieved from California, USA:

ISO. (1994). *ISO 7730: Moderate Thermal Environments-Determination of the PMV and PPD Indices and Specification of the Conditions for Thermal Comfort*. Geneva: ISO.

Jendritzky, G., De Dear, R., & Havenith, G. (2012). UTCI -- Why another thermal index? *International Journal of Biometeorology, 56*(3), 421-428.

Jendritzky, G., & Nübler, W. (1981). A model analysing the urban thermal environment in physiologically significant terms. *Archives for meteorology, geophysics, and bioclimatology, Series B, 29*(4), 313-326.

Kramer, M. G. (2013). *Our built and natural environments: a technical review of the interactions among land use, transportation, and environmental quality*. Retrieved from Washington, DC, United States: http://www.epa.gov/smartgrowth/pdf/b-and-n/b-and-n-EPA-231K13001.pdf

Lang, J., Cheng, S., Wei, W., Zhou, Y., Wei, X., & Chen, D. (2012). A study on the trends of vehicular emissions in the Beijing–Tianjin–Hebei (BTH) region, China. *Atmospheric environment, 62*, 605-614.

Long, Y., & Liu, X. (2013). Automated identification and characterization of parcels (AICP) with OpenStreetMap and Points of Interest. *Beijing City Lab, Working paper # 16*.

Marchettini, N., Brebbia, C. A., Pulselli, R., & Bastianoni, S. (2014). *The Sustainable City IX: Urban Regeneration and Sustainability* (Vol. 191): WIT press.

Martins, T. A., Adolphe, L., Bonhomme, M., Bonneaud, F., Faraut, S., Ginestet, S., Michel, C., & Guyard, W. (2016). Impact of Urban Cool Island measures on outdoor climate and pedestrian comfort: simulations for a new district of Toulouse, France. *Sustainable Cities and Society, 26*, 9-26.

Matzarakis, A., Rutz, F., & Mayer, H. (2007). Modelling Radiation fluxes in simple and complex environments - Application of the RayMan model. *International Journal of Biometeorology, 51*, 323-334.

Matzarakis, A., Rutz, F., & Mayer, H. (2010). Modelling Radiation fluxes in simple and complex environments - Basics of the RayMan model. *International Journal of Biometeorology, 54*, 131-139.

Morakinyo, T. E., & Lam, Y. F. (2016). Simulation study of dispersion and removal of particulate matter from traffic by road-side vegetation barrier. *Environmental Science and Pollution Research, 23*(7), 6709-6722.

Mueller, N., Rojas-Rueda, D., Basagaña, X., Cirach, M., Cole-Hunter, T., Dadvand, P., Donaire-Gonzalez, D., Foraster, M., Gascon, M., & Martinez, D. (2017). Urban and transport planning related exposures and mortality: a health impact assessment for cities. *Environmental health perspectives, 125*(1), 89.

Nasrollahi, N., Hatami, M., Khastar, S. R., & Taleghani, M. (2017). Numerical evaluation of thermal comfort in traditional courtyards to develop new microclimate design in a hot and dry climate *Sustainable Cities and Society, 35*, 449-467.

National Bureau of Statistics of China. (2008). *2008 Time Use Survey in China*. Beijing, China: China Statistics Press.

National Bureau of Statistics of China. (2010). *Tabulation on the 2010 Population Census of the People's Republic of China*. Beijing, China: China Statistics Press and Beijing Info Press.

National Health Commission of China. (2015). *Report on Chinese Residents' Chronic Diseases and Nutrition*. Retrieved from Beijing, China: http://www.chinadaily.com.cn/m/chinahealth/2015-06/15/content_21008408.htm

Ntziachristos, L., Samaras, Z., Eggleston, S., Gorissen, N., Hassel, D., & Hickman, A. (2000). *Copert III. Computer Programme to calculate emissions from road transport, methodology and emission factors (version 2.1)*. Retrieved from Copenhagen: https://www.eea.europa.eu/publications/Technical_report_No_49

Ooka, R. (2007). Recent development of assessment tools for urban climate and heat‐island investigation especially based on experiences in Japan. *International Journal of Climatology: A Journal of the Royal Meteorological Society, 27*(14), 1919-1930.

Ravazzoli, E., & Torricelli, G. P. (2017). Urban mobility and public space. A challenge for the sustainable liveable city of the future. *The Journal of Public Space, 2*(2), 37-50.

Ren, G., Chu, Z., Chen, Z., & Ren, Y. (2007). Implications of temporal change in urban heat island intensity observed at Beijing and Wuhan stations. *Geophysical Research Letters, 34*(5).

Robinson, D. (2012). *Computer modelling for sustainable urban design: Physical principles, methods and applications*: Routledge.

Rozos, E., Makropoulos, C., & Maksimović, Č. (2013). Rethinking urban areas: an example of an integrated blue-green approach. *Water Science and Technology: Water Supply, 13*(6), 1534-1542.

Sailor, D. J. (2011). A review of methods for estimating anthropogenic heat and moisture emissions in the urban environment. *International Journal of Climatology, 31*(2), 189-199.

Sailor, D. J., & Lu, L. (2004). A top–down methodology for developing diurnal and seasonal anthropogenic heating profiles for urban areas. *Atmospheric environment, 38*(2004), 2737-2748.

Salata, F., Golasi, I., de Lieto Vollaro, R., & de Lieto Vollaro, A. (2016). Urban microclimate and outdoor thermal comfort. A proper procedure to fit ENVI-met simulation outputs to experimental data. *Sustainable Cities and Society, 26*, 318-343.

Samaras, C., Tsokolis, D., Toffolo, S., Garcia-Castro, A., Vock, C., Ntziachristos, L., & Samaras, Z. (2014). *Limits of applicability of COPERT model to short links and congested conditions.* Paper presented at the 20th International Transport and Air Pollution Conference.

Shirehjini, R. M. (2016). *Integrating environmentally sustainable design principles into livable neighborhood.* Paper presented at the Proceedings of the 1st International Conference on Sustainable Buildings and Structures.

Shooshtarian, S., Rajagopalan, P., & Sagoo, A. (2018). A comprehensive review of thermal adaptive strategies in outdoor spaces. *Sustainable Cities and Society*.

Simon, H. (2016). *Modeling urban microclimate: development, implementation and evaluation of new and improved calculation methods for the urban microclimate model ENVI-met.* (Doctoral dissertation), Johannes Gutenberg-Universität Mainz.

Skiena, S. S. (1998). *The Algorithm Design Manual*: Springer Science & Business Media.

Smit, R., Brown, A., & Chan, Y. (2008). Do air pollution emissions and fuel consumption models for roadways include the effects of congestion in the roadway traffic flow? *Environmental Modelling & Software, 23*(10-11), 1262-1270.

Su, J. G., Apte, J. S., Lipsitt, J., Garcia-Gonzales, D. A., Beckerman, B. S., De Nazelle, A., Texcalac-Sangrador, J. L., & Jerrett, M. (2015). Populations potentially exposed to traffic-related air pollution in seven world cities. *Environment international, 78*, 82-89.

The Weather Channel. Weather Underground. Retrieved 2019.2.24 https://www.wunderground.com/history/daily/cn/beijing/ZBAA/date/2017-2-24

Townsend, H. (2016). *Active Communities Travel Planning -- Literature Review*. Retrieved from Wellington, New Zealand: http://www.gw.govt.nz/assets/Transport/Sustainable-Transport-2012/Active-Communities-Review.pdf

United Nations. (2013). *Streets as public spaces and drivers of urban prosperity*. UN Habitat.

Van Dam, K., Bustos-Turu, G., & Shah, N. (2017). *A methodology for simulating synthetic populations for the analysis of socio-technical infrastructures.* Paper presented at the Advances in Social Simulation 2015.

Van Dam, K., Nikolic, I., & Lukszo, Z. (2013). *Agent-Based Modelling of Socio-Technical Systems* (Vol. 9). Dordrecht: Springer Netherlands

Vardoulakis, S., Fisher, B. E., Pericleous, K., & Gonzalez-Flesca, N. (2003). Modelling air quality in street canyons: a review. *Atmospheric environment, 37*(2), 155-182.

Wang, H., Fu, L., Zhou, Y., Du, X., & Ge, W. (2010). Trends in vehicular emissions in China's mega cities from 1995 to 2005. *Environmental Pollution, 158*(2), 394-400.

Wania, A., Bruse, M., Blond, N., & Weber, C. (2012). Analysing the influence of different street vegetation on traffic-induced particle dispersion using microscale simulations. *Journal of environmental management, 94*(1), 91-101.

Waraich, R. A., Charypar, D., Balmer, M., Axhausen, K. W., Waraich, R. A., Waraich, R. A., Axhausen, K. W., & Axhausen, K. W. (2009). *Performance improvements for large scale traffic simulation in MATSim.* Paper presented at the 9th Swiss Transport Research Conference, Ascona.

Wise, S., Crooks, A., & Batty, M. (2017). Transportation in Agent-Based Urban Modelling. In M.-R. Namazi-Rad, L. Padgham, P. Perez, K. Nagel, & A. Bazzan (Eds.), *Agent Based Modelling of Urban Systems: First International Workshop, ABMUS 2016, Held in Conjunction with AAMAS, Singapore, Singapore, May 10, 2016, Revised, Selected, and Invited Papers* (pp. 129-148). Cham: Springer International Publishing.

Wong, N. H., & Peck, T. T. (2005). The impact of vegetation on the environmental conditions of housing estates in Singapore. *International Journal on Architectural Science, 6*(1), 31-37.

Woodcock, J., Edwards, P., Tonne, C., Armstrong, B. G., Ashiru, O., Banister, D., Beevers, S., Chalabi, Z., Chowdhury, Z., & Cohen, A. (2009). Public health benefits of strategies to reduce greenhouse-gas emissions: urban land transport. *The Lancet, 374*(9705), 1930-1943.

Yang, L., Van Dam, K., Anvari, B., & De Nazelle, A. (forthcoming). Simulating the impact of urban transport infrastructure design on local air quality in Beijing *Social Simulation for a Digital Society: Applications and Innovations in Computational Social Science*: Springer International Publishing AG, Cham, in press.

Yang, X., Zhao, L., Bruse, M., & Meng, Q. (2013). Evaluation of a microclimate model for predicting the thermal behavior of different ground surfaces. Building and Environment, 60, 93-104.

Zhang, B., Xie, G., Xia, B., & Zhang, C. (2012). The effects of public green spaces on residential property value in Beijing. *Journal of Resources and Ecology, 3*(3), 243-253.

Zhang, Y., Wu, L., Zou, C., Jing, B., Li, X., Barlow, T., Kevin, T., André, M., Liu, Y., & Ren, P. (2017). Development and application of urban high temporal-spatial resolution vehicle emission inventory model and decision support system. *Environmental Modeling & Assessment, 22*(5), 445-458.

Zhang, Z., Ma, J., & Lei, Y. (2011). Beijing electric power load and its relation with meteorological factors in summer. *Journal of Applied Meteorological Science, 22*(6), 760-765.

[1] Climate-sensitive (or responsive) urban design implies that urban spaces are designed with considering the essential components of microclimate such as air temperature and wind environment and can mitigate stressed local conditions and reduce pollution to the natural environment (Marchettini et al., 2014).

[2] Thermal comfort can be defined as individuals' satisfaction with the thermal environment (ASHRAE, 2010).

[3] Universal Thermal Climate Index was defined as "the isothermal air temperature of the reference condition that would elicit the same dynamic response (strain) of the physiological model" (Jendritzky et al., 2012).